

1 **Long-term trends of surface ozone and its influencing factors at**
2 **the Mt. Waliguan GAW station, China, Part 1: Overall trends and**
3 **characteristics.**

4 **W. Y. Xu¹, W. L. Lin², X. B. Xu^{1,*}, J. Tang², J.Q. Huang³, H. Wu³, X.C.Zhang²**

5

6 [1] State Key Laboratory of Severe Weather & Key Laboratory for Atmospheric Chemistry
7 of China Meteorology Administration, Chinese Academy of Meteorological Sciences, Beijing,
8 China

9 [2] Meteorological Observation Center, China Meteorological Administration, Beijing, China

10 [3] Waliguan Observatory, Qinghai Meteorological Bureau, Xining, China

11 * Correspondence to: X. B. Xu (xuxb@cams.cma.gov.cn)

12

13 **Abstract**

14 Tropospheric ozone is an important atmospheric oxidant, greenhouse gas and atmospheric
15 pollutant at the same time. The oxidation capacity of the atmosphere, climate, human and
16 vegetation health can be impacted by increasing of the ozone level. Therefore, long-term
17 determination of trends of baseline ozone is highly needed information for environmental and
18 climate change assessment. So far, studies on the long-term trends of ozone at representative
19 sites are mainly available for European and North American sites. Similar studies are lacking
20 for China and many other developing countries. Measurements of surface ozone were carried
21 out at a global baseline Global Atmospheric Watch (GAW) station in the north-eastern
22 Tibetan Plateau region (Mt. Waliguan, 36°17' N, 100°54' E, 3816m a.s.l.) for the period of
23 1994 to 2013. To uncover the variation characteristics, long-term trends and influencing
24 factors of surface ozone at this remote site in western China, a two-part study has been carried
25 out, with this part focusing on the overall characteristics of diurnal, seasonal and long-term
26 variations and the trends of surface ozone. To obtain reliable ozone trends, we performed the
27 Mann-Kendall trend test and the Hilbert-Huang Transform (HHT) analysis on the ozone data.
28 Our results confirm that the mountain-valley breeze plays an important role in the diurnal
29 cycle of surface ozone at Waliguan, resulting in higher ozone values during the night and

1 lower ones during the day, as was previously reported. Systematic diurnal and seasonal
2 variations were found in mountain-valley breezes at the site, which were used in defining
3 season-dependent daytime and nighttime periods for trend calculations. Significant positive
4 trends in surface ozone were detected for both daytime (0.24 ± 0.16 ppbv yr⁻¹) and nighttime
5 (0.28 ± 0.17 ppbv yr⁻¹). The largest nighttime increasing rate occurred in autumn
6 (0.29 ± 0.11 ppbv yr⁻¹), followed by spring (0.24 ± 0.12 ppbv yr⁻¹), summer (0.22 ± 0.20 ppbv yr⁻¹)
7 and winter (0.13 ± 0.10 ppbv yr⁻¹), respectively. The HHT spectral analysis identified four
8 different stages with different positive trends, with the largest increase occurring around May
9 2000 and Oct. 2010. The HHT results suggest that there were 2-4a, 7a and 11a periodicities in
10 the timeseries of surface ozone at Waliguan. The results of this study can be used for
11 assessments of climate and environment change and in the validation of chemistry-climate
12 models.

13

14 **1 Introduction**

15 Ozone (O₃) is one of the key atmospheric species and is closely related to climate change and
16 environmental issues (IPCC, 2013). The stratospheric ozone layer protects living organisms at
17 the Earth's surface against the harmful solar UV radiation, while tropospheric ozone is an
18 important greenhouse gas and governs oxidation processes in the Earth's atmosphere through
19 formation of OH radical (Monks et al., 2015;The Royal Society, 2008;Young et al.,
20 2013;Lelieveld and Dentener, 2000;Levy, 1971). In the surface layer, ozone is also one of the
21 toxic gases for human beings and vegetation.

22 Data on the spatiotemporal variations of ozone are greatly needed for assessing the impacts of
23 ozone on human health, ecosystems, and climate. Since ozone is a secondary pollutant, with
24 a lifetime of 22 days (Young et al., 2013), its mixing ratios are influenced both by local
25 photochemistry and by transport of ozone and its precursors (Wang et al., 2006a;Lal et al.,
26 2014). Deep convection and stratosphere-to-troposphere exchange (STE) events can also
27 bring down ozone-rich air from above and influence surface ozone mixing ratios at high-
28 elevation sites (Stohl et al., 2003;Lefohn et al., 2012;Jia et al., 2015;Ma et al., 2014;Langford
29 et al., 2015;Lin et al., 2015a). In the troposphere, particularly in the surface layer, ozone is
30 highly variable in space and time due to the large variabilities of its dominant sources and
31 sinks, which are impacted by anthropogenic activities and meteorological conditions. So far,

1 there has been no better way than networked monitoring to obtain the spatial distribution and
2 long-term temporal variation of surface ozone.

3 The Global Atmosphere Watch (GAW) programme of the World Meteorological
4 Organization (WMO) has been one of the key international initiatives in long-term monitoring
5 of the chemical and physical properties of the atmosphere. Many GAW stations have been set
6 up to monitor atmospheric compositions including surface ozone due to its importance and
7 due to the urgent need to evaluate the trends of baseline ozone. Based on data from some
8 GAW sites and other sources, past trends in surface baseline ozone have been reported for
9 Europe and North America (Cui et al., 2011; Gilge et al., 2010; Oltmans et al., 2013; Vingarzan,
10 2004; Parrish et al., 2012; Logan et al., 2012), which mostly reveal strong increases in ozone
11 before 2000 and slow or even no growth afterwards. Data from some important regions, e.g.,
12 East Asia and South America, are very scarce, which makes them even more valuable. China,
13 as one of the rapidly developing countries, is contributing increasing ozone precursor
14 emissions to the atmosphere and transport from the South and East Asian sector was thought
15 to be most responsible for the increase in ozone in the western United States (Cooper et al.,
16 2010), though other studies suggest that STE events had an equivalent important role in
17 causing high-ozone events at western U.S. alpine sites during spring (e.g. Langford et al.,
18 2009; Ambrose et al., 2011; Lin et al., 2012a; Lin et al., 2015a). A recent study by Lin et al.
19 (2015b) found that although rising Asian emissions contributed to increasing springtime
20 baseline ozone over the western U.S. from the 1980s to the 2000s, the observed western US
21 ozone trend over the short period of 1995-2008 previously reported by Cooper et al. (2010)
22 was strongly biased by meteorological variability and measurement sampling artefacts,
23 resulting in an overestimate of the trend. Extending the analysis to 1995–2014, a weaker
24 ozone trend of 0.31 ± 0.21 ppbv yr⁻¹ was found from observations and a similar one from
25 model results. Nevertheless, the impact of Asian pollution outflow events on western US
26 surface ozone is evident (Lin et al., 2012; Lin et al., 2015a).

27 Besides the impact of Asian pollution outflow on the surface ozone in other regions, it is at
28 least equally important to know how the level of surface ozone in Asia, particular in China,
29 has been changing. Long-term changes in ozone in China, however, have only been reported
30 in a few publications. Ding et al. (2008) studied the tropospheric ozone climatology over
31 Beijing based on data from the MOZAIC (Measurement of Ozone and Water Vapor by
32 Airbus In-Service Aircraft) program and found a 2% yr⁻¹ increase of boundary layer ozone

1 from the period of 1995-1999 to 2000-2005 over Beijing in the North China Plain (NCP)
2 region and a weaker increasing trend of free-tropospheric ozone. Wang et al. (2012) reported
3 a similar increasing trend of lower tropospheric ozone and larger ozone increases in the
4 middle and upper troposphere for the period of 2002-2010 based on ozonesonde
5 measurements over Beijing. Ma et al. (2016) found an increase of 1.1 ppbv yr⁻¹ for the period
6 2003-2015 in the maximum daily average 8 h concentration of ozone at Shangdianzi, a
7 background site in the NCP. Xu et al. (2008) reported positive trends of extreme values and
8 increased variability in 6 periods of ozone measurements from 1991 to 2006 at Lin'an, a
9 background site in the Yangtze River Delta (YRD) region. Wang et al. (2009) found a
10 significant increasing trend of 0.58 ppbv yr⁻¹ during 1994-2007 at a coastal site of Hong Kong
11 in the Pearl River Delta (PRD) region, which was caused by rapid increases in ozone
12 precursor emissions in the upwind source regions. The above studies all focus on the most
13 polluted regions in the eastern part of China, i.e., the NCP, YRD and PRD, aiming to study
14 the impact of growing precursor emissions on ozone trends. The trend of ozone over remote
15 regions in China still remains to be studied based on long-term observations.

16 Continuous long-term observations of surface ozone have been made only at a few
17 representative sites in China, among which is the Mt. Waliguan (WLG) GAW station, which
18 has the longest ozone measurement record in China. It is a pristine high elevation site located
19 downwind of the European, Central Asian and Indian outflow, representative of the baseline
20 of Eurasia. A few studies have already been performed on short-term measurements of ozone
21 at WLG. Surface ozone at the site has been proved to be highly representative of free-
22 tropospheric ozone (Ma et al., 2002b) and hence is subjected to the influences of STE events
23 (Ding and Wang, 2006;Zhu et al., 2004). Air masses from the west are dominant at WLG and
24 were found to be associated with the highest ozone mixing ratios (Wang et al., 2006b). Only
25 in summer a substantial portion of the airflows comes from the eastern sector and exposes the
26 surface ozone mixing ratio to some regional anthropogenic influences (Wang et al.,
27 2006b;Xue et al., 2011). Previous studies of ozone at WLG, based on short-term
28 measurements and modelling results, clarified the causes for certain episodes or for the
29 diurnal and seasonal cycles of ozone (Ma et al., 2002a;Ma et al., 2005;Zhu et al., 2004). The
30 overall variation characteristics and long-term trend of ozone at WLG have not yet been
31 studied. Considering the geographical representativeness of the WLG site, results on the long-
32 term variations of ozone at WLG may improve understanding of ozone changes in the
33 northern mid-latitudes, particularly in the rural and remote regions of Eurasia.

1 The most common method used in the detection of ozone trends is the linear least squares
2 method (Tarasova et al., 2009;Cui et al., 2011;Wang et al., 2009;Xu et al., 2008). Other
3 studies directly compared mean ozone levels of different periods to detect possible trends
4 (Ding et al., 2008;Lin et al., 2014). Oltmans et al. (2013) determined trends and their
5 significance in the W126 and W_Low metrics using the Theil-Sen estimate together with the
6 Mann-Kendall's tau test (Kendall, 1955;Sen, 1968). The non-linear variation of ozone mixing
7 ratio with season and many other meteorological factors can introduce uncertainties into the
8 linear trend analysis. Wang et al. (2012) deseasonalized the monthly data by subtracting the
9 average of all monthly data for a given month from the original data of the same month before
10 performing a linear regression analysis. Oltmans et al. (2006) and Oltmans et al. (2013) first
11 performed an autoregressive model fitting incorporating explanatory variables (that are
12 known sources of ozone variability) and a cubic polynomial fit to better represent the long-
13 term variations of ozone, then used a bootstrap method to determine the trends of ozone.
14 However, surface ozone typically is influenced by many factors, which makes it hard to
15 determine which to incorporate. The seasonal Mann-Kendall test, which is a modified version
16 of the non-parametric Mann-Kendall trend test, can account for the seasonal variation within
17 the data Hamed and Ramachandra Rao (1998). It has been widely applied in hydrology and
18 seldom in atmospheric chemistry. The Hilbert-Huang Transform (HHT) analysis, which has
19 been widely applied on the analysis of meteorological datasets and not yet on that of
20 atmospheric composition data, is a precise and adaptive spectral analysis method, that can
21 divide the signal into various oscillation modes and study the anomaly and periodicity within
22 the data (Rao and Hsu, 2008). Applications of HHT on temperature, wind, rainfall and solar
23 radiation data have proved that the HHT method is capable of capturing synoptic and climatic
24 features, revealing known diurnal, seasonal, annual and inter-annual cycles (Huang, 2014).

25 In this paper, we present the first part of an analysis on 20-year surface ozone mixing ratio at
26 WLG, focusing mainly on the overall, diurnal, seasonal and long-term variations
27 characteristics and the trends of surface ozone. We apply a linear regression as well as a
28 seasonal Mann-Kendall test together with the Theil-Sen estimate to calculate the overall trend
29 of ozone. The HHT spectral analysis method is used for the first time to investigate the ozone
30 trends during different periods and the underlying anomalies and periodicities within the
31 ozone data. A detailed discussion on the influencing factors contributing to the ozone
32 variation at WLG will be presented in a companion paper.

1

2 **2 Data and Methodology**

3 **2.1 Site and Measurements**

4 The Mt. Waliguan site (WLG, 36°17' N, 100°54' E, 3816 m asl) is located in Qinghai
5 Province, China. It is one of the global baseline stations of the WMO/GAW network and the
6 only one in the hinterland of the Eurasian continent. WLG is situated at the northeast edge of
7 the Qinghai-Tibetan Plateau and surrounded by highland steppes, tundra, deserts, salt lakes,
8 etc. (Fig.1). With very low population (about 6 persons km⁻²) and hardly any industry within
9 30 km, the WLG site is far from major anthropogenic sources of ozone precursors. However,
10 some impact of long-range transport of anthropogenic pollutants from the NE-SE sector
11 cannot be excluded, particularly from the major cities Xining (about 90 km northeast of WLG,
12 population ~2.13 millions) and Lanzhou (about 260 km east of WLG, population ~3.1
13 millions). Such impact, if any, may be significant only during the warmer period (May-
14 September), as suggested by previous air mass trajectory studies (Zhang et al., 2011). The
15 vehicle emission on the highway running from the northwest to the northeast of WLG may
16 also be another source for anthropogenic ozone precursors (Wang et al., 2015).

17 The WLG baseline station was established in 1994. The long-term monitoring program for
18 surface ozone began in August 1994. The mixing ratios of surface ozone have been measured
19 using two ozone analysers (Model 49, Thermal Environmental Instruments; one of the
20 analysers was replaced with a Model 49i ozone analyser in 2011) at a sampling height of 7
21 meters. The analysers have been automatically zeroed alternatively every second day by
22 introducing ozone-free air for 45 min. Seasonal multipoint calibrations (8 points) have been
23 conducted using an ozone calibrator (Model 49PS, Thermal Environmental Instruments). The
24 analysers have been checked weekly for changes in instrument parameters. The inlet filters
25 have been replaced weekly. Maintenance on the observation system has been performed
26 yearly and whenever it was necessary. The yearly maintenance includes cleaning of
27 absorption tubes, pumps, inlet tubing and other connecting parts, and checking of the inlet
28 loss. In the years 1994, 1995, 2000, 2004, and 2009, the ozone calibrator and analysers at
29 WLG were compared with the transfer standard from the WMO World Calibration Centre for
30 Surface Ozone and Carbon Monoxide, EMPA Dübendorf, Switzerland. Intercomparison
31 results show excellent or good agreement between the WLG instruments and the transfer

1 standard (Zellweger et al., 2000;Zellweger et al., 2004;Zellweger et al., 2009). The two
2 instruments performed parallel measurements, recording surface ozone data as 5-minute
3 averages, which were corrected annually based on the zero-checks and multipoint calibrations.
4 If the observed ozone values from the two analysers agreed within 3 ppb, average values were
5 calculated and included in the final dataset. Otherwise, causes for the differences were
6 searched by the principal investigator and only data from the well-performing analyser were
7 included in the dataset. 95% of the data pairs show discrepancies within ± 1.0 ppb and the
8 difference between two instruments shows a nearly random distribution around zero. 5-minute
9 averaged ozone mixing ratios from Aug. 1994 to Dec. 2013 were then averaged into hourly
10 data and used in this study. In the trend analysis, monthly average ozone mixing ratios were
11 acquired by first calculating the daily average ozone values and then performing a monthly
12 averaging. A data completeness of 75% was required for each averaging step.

13 Meteorological observations have been made at the site using automatic weather stations
14 (AWS) installed on the ground level and on an 80 m tower at 2, 10, 20, 40 and 80 m height.
15 These observations provide meteorological parameters such as temperature, pressure,
16 precipitation, and wind speed/direction in 5 min resolution. Additionally, the vertical velocity
17 is measured at the 80 m platform. The 10 m horizontal wind and 80 m vertical wind data from
18 Aug. 1994 to Dec. 2013 are used in this study and have been accordingly averaged into hourly
19 data, which meet a data completeness requirement of 75%.

20

21 **2.2 Determination of daytime and nighttime**

22 Past research has already revealed that the surface ozone at WLG is governed by different air
23 masses during daytime and nighttime (Ma et al., 2002b). The WLG station experiences
24 upslope winds during the day and is influenced by boundary layer (BL) air, while during the
25 night, winds are downslope and the site is controlled by free tropospheric (FT) air. The
26 boundary layer air is largely influenced by local photochemistry and may contain pollutants
27 transported from nearby areas, while the free-tropospheric air may sometimes contain signals
28 of long-range transport or STE events. Hence, it is of necessity to differentiate between
29 daytime and nighttime ozone mixing ratios in order to study the trends associated with
30 different air masses.

1 In the previous study (Xu et al., 2011), daytime and nighttime were defined as fixed time
2 ranges (e.g. 11:00-16:00 LT for daytime and 23:00-4:00 LT for nighttime). However, the
3 actual well-developed day and night time ranges vary with season, and so does the local wind.
4 Figures 2a-c respectively show the season-diurnal variation characteristics of 10 m zonal (u)
5 and meridional (v) wind velocity and the 80 m vertical (w) wind velocity. Due to the local
6 topography, the WLG station is under the influence of mountain-valley breezes and all three
7 wind vectors exhibit distinct diurnal variation characteristics. The height difference to the
8 west of Mt. WLG is much larger than that to the east, hence valley breezes during daytime
9 come from the west accompanied by upward drafts, resulting in a diurnal maximum u and w
10 vector between noontime and middle afternoon depending on the season. The v vector
11 changes from southern to northern winds around noontime. Mountain breezes during the night
12 come from the south-east sector accompanied by subsiding air flows, resulting in low u and w
13 and high v during the night. The dominant air flow at WLG is westerly during the cold
14 seasons, which enhances the westerly valley breeze during the day and cancels out the
15 easterly mountain breeze during the night. During the warm seasons, easterly winds gain in
16 frequency, which sometimes cancels out the daytime valley breeze and enhances the
17 nighttime mountain breeze. The distinct diurnal variation of the wind can be used to define a
18 daytime and nighttime range that varies with season. The white dots in Fig.2 represent the
19 monthly average occurrence hour of the diurnal maximum u . In this study, a 6 hour time
20 range that is centred around the white dots is used as the daytime range (white dashed lines in
21 Fig. 2). The nighttime window also covers 6 hours and is considered to be offset by 12 hours
22 to the daytime window.

23

24 **2.3 Trend analysis**

25 The trend analysis is performed using both the spearman's linear trend analysis and the
26 modified Mann-Kendall trend test. The Mann-Kendall test is performed using a Fortran
27 program developed by Helsel et al. (2006). Here, a brief description on the modified Mann-
28 Kendall test is given. The Mann-Kendall test is a non-parametric test commonly used to
29 detect trends. Hamed and Ramachandra Rao (1998) modified the test, so that it can be used on
30 data with seasonality.

1 For two sets of observations $X = x_1, x_2, \dots, x_n$ and $Y = y_1, y_2, \dots, y_n$, the rank correlation test
 2 as proposed by (Kendall, 1955) is performed as the following:

$$3 \quad S = \sum_{i < j} a_{ij} b_{ij} \quad (1)$$

$$4 \quad \text{Where } a_{ij} = \text{sign}(x_j - x_i) = \begin{cases} 1 & x_i < x_j \\ 0 & x_i = x_j \\ -1 & x_i > x_j \end{cases} \text{ and } b_{ij} \text{ is the equivalent for } Y. \quad (2)$$

5 If Y is replaced with the time order $T = 1, 2, \dots, n$, the test becomes a trend test and $S =$
 6 $\sum_{i < j} a_{ij}$. The significance of the trend is tested by comparing the standardized test statistic
 7 $Z = S / \sqrt{\text{var}(S)}$ to the standard normal variate at a given significance level (Z_α). Here, a
 8 modified $\text{var}(S)$ is given by:

$$9 \quad \text{var}(S) = \frac{n(n-1)(2n+5)}{18} \frac{n}{n_S^*}, \quad (3)$$

10 where $\frac{n}{n_S^*}$ represents a correction for the autocorrelation that exists in the data and can be
 11 obtained by an approximation to the theoretical values.

$$12 \quad \frac{n}{n_S^*} = 1 + \frac{2}{n(n-1)(n-2)} \sum_{i=1}^n (n-i)(n-i-1)(n-i-2) \rho_s(i) \quad (4)$$

13 Here $\rho_s(i)$ is the autocorrelation function of the ranks of the observations.

14 If $|Z| > Z_{1-\alpha/2}$, then the data is non-stationary, a positive Z indicates a positive trend and a
 15 negative Z suggests a declining trend. If $|Z| \leq Z_{1-\alpha/2}$, then the data is stationary. Here we use
 16 $\alpha = 0.05$, hence the corresponding critical $Z_{1-\alpha/2} = 1.96$. A non-parametric method (Theil-Sen
 17 estimate) is then used to estimate the magnitude of the trend, details can be found in Sen
 18 (1968).

19

20 **2.4 The Hilbert-Huang Transform analysis**

21 The Hilbert-Huang Transform (HHT) analysis is a combination of the Empirical Mode
 22 Decomposition (EMD) and the Hilbert Spectral analysis proposed by Huang et al. (1998). It is
 23 often used to analyse the time-frequency variation of non-linear and non-stationary processes.
 24 The EMD acts as a time-frequency filter, it decomposes the data into several oscillation
 25 modes with different characteristic time scales. The HHT method has been proved to be an
 26 efficient and precise method in investigating the periodicity, long-term oscillations and trends

1 that are embedded within the data (Huang and Wu, 2008). So far, it has been widely applied
 2 in the studies of meteorology and climate, including wind field, temperature, radiation and
 3 rainfall analysis (Rao and Hsu, 2008;Lundquist, 2003;El-Askary et al., 2004), but it has not
 4 been used on atmospheric composition data. Here we give a brief description of the HHT
 5 method.

6 First, the EMD is performed on the data, to decompose the data into n intrinsic mode
 7 functions (IMF), c_1, c_2, \dots, c_n , and one residual r_n , which are ordered from the smallest to the
 8 largest variation time scale (Huang et al., 2003).

$$9 \quad x(t) = \sum_{j=1}^n c_j + r_n \quad (5)$$

10 Then the Hilbert transform is applied to each IMF using Eq. 6,

$$11 \quad y(t) = \frac{1}{\pi} P \int_{-\infty}^{\infty} \frac{x(t')}{t-t'} dt', \quad (6)$$

12 where P is the Cauchy principal value. An analytical signal is then obtained with Eq.7,

$$13 \quad z(t) = x(t) + iy(t) = a(t)e^{i\theta(t)}, \quad (7)$$

$$14 \quad \text{where, } a(t) = [x^2(t) + y^2(t)]^{1/2} \text{ and } \theta(t) = \arctan\left(\frac{y(t)}{x(t)}\right). \quad (8)$$

15 The instantaneous frequency ω can be calculated as the following:

$$16 \quad \omega(t) = \frac{d\theta(t)}{dt}. \quad (9)$$

17 Thus, Eq.5 can be transformed into the following expression:

$$18 \quad x(t) = \Re \sum_{j=1}^n a_j(t) \exp(i \int \omega_j(\tau) d\tau), \quad (10)$$

19 where \Re is the real part of the complex number.

20 To obtain the Hilbert amplitude spectrum $H(\omega, t)$, we assign for each time t , the calculated
 21 amplitude $a_j(t)$ to the associated $\omega_j(t)$. An integration of $H(\omega, t)$ over the frequency span yields
 22 the instantaneous energy (IE), which represents the time variation of the energy. An
 23 integration along the time span yields the marginal Hilbert spectrum $h(\omega)$, which provides
 24 information on how the frequency is distributed over the entire span.

25 The degree of stationarity $DS(\omega)$ is often used to investigate the stationarity and periodicity of
 26 the data, it is defined as:

$$27 \quad DS(\omega) = \frac{1}{T} \int_0^T \left(1 - \frac{H(\omega, t)}{h(\omega)/T}\right)^2 dt, \quad (11)$$

1 where T is the entire time span.

2 The volatility $V(t, T)$ is defined as the ratio of the sum of certain IMF components $S_h(t)$ to the
3 original signal $S(t)$. Here we use the summation of residual and all the IMFs except for the
4 first one as $S_h(t)$:

$$5 \quad V(t, T) = \frac{S_h(t)}{S(t)} = \frac{\sum_{j=2}^n c_j(t) + r(t)}{S(t)}, \quad (12)$$

6 where n is the number of IMFs.

7 **2.5 The gap-filling of the monthly average ozone data**

8 To perform the HHT analysis, a complete, even-spaced data series is required. Hence we need
9 to fill the gaps in the monthly average surface ozone mixing ratio data. In our monthly ozone
10 time series, gaps of one to six months can be found in 1997, 1998, 1999 and 2002. If the gap
11 is small and occurs in between the ozone seasonal low and peak value, then a spline
12 interpolation suffices. However, this is not the case for some gaps. In 1997 and 1998, the gaps
13 occurred during summertime, when the seasonal peak of ozone mixing ratio was expected. In
14 2002, the gap continued on to winter, when the lowest ozone mixing ratio was expected. A
15 simple spline interpolation would have underestimated the seasonal peak value and
16 overestimated the seasonal low. Hence, we applied the following method to fill the gaps.

17 First, the monthly mean ozone timeseries from 1994 to 2013 is shaped into an array $O_3(i, j)$ of
18 the size [20 years \times 12 months], where $i=1994, \dots, 2013$ and $j=1, \dots, 12$.

19 The gaps in $O_3(i, j)$ are filled by applying a spline interpolation on each row of the array:

$$20 \quad O_{3,spline}(1994, \dots, 2013, j) = spline(O_3(1994, \dots, 2013, j)), j = 1, \dots, 12 \quad (13)$$

21 In this way, both the average value of ozone mixing ratio at a certain month and the overall
22 ozone trend will be considered. A complete dataset of average monthly ozone mixing ratio
23 can then be recreated by using interpolated data only on months of missing observation data:

$$24 \quad O_{3,complete} = \begin{cases} O_{3,spline}, & \text{missing } O_3 \\ O_3, & \text{existing } O_3 \end{cases} \quad (14)$$

25 Our method could yield a reasonable interpolated timeseries with both seasonal low and peak
26 values occurring at the right time of year.

1 **3 Results and Discussion**

2 **3.1 Season-diurnal variation characteristics of ozone**

3 The average season-diurnal variation of surface ozone during 1994-2013 is displayed in Fig.
4 3Figure 3 with the monthly average local times associated with the diurnal minimum ozone
5 and maximum zonal wind. The seasonal maximum ozone occurs during summer, with an
6 average peak in June-July, while the minimum is found in winter (Fig. 3a), which will be
7 discussed in detail in Section 3.2.

8 Daily maximum ozone usually occurs during nighttime, while the daily minimum ozone is
9 found around noontime, on average at 12 am, Beijing Local Time (Fig. 3c). Ma et al. (2002b)
10 suggest that the WLG station is mostly influenced by boundary layer (BL) air that is brought
11 up through an upslope flow during the day, while a downslope flow brings down free
12 tropospheric (FT) air during the night. The BL air masses are typically characterised by lower
13 ozone mixing ratios in comparison with FT air masses, hence the occurrence of the daily
14 ozone minimum value indicates the time when the BL is fully developed and the air within is
15 well mixed.

16 From Fig. 3b it can be denoted that, the occurrence time of the daily minimum ozone mixing
17 ratio (red dots) shows a significant annual variation similar to that of the maximum zonal
18 wind velocity (white dots), with the former occurring 1-2 hours earlier than the later. Due to
19 the annual variation of the BL development, the daily minimum ozone should occur earlier in
20 the day during warm seasons and later in the day during cold seasons. This phenomenon can
21 indeed be confirmed by Fig. 3b, however, the ozone minimum of June-August seems to occur
22 later than expected. This phenomenon is not seen in the season-diurnal variation of horizontal
23 or vertical wind speeds, indicating that it is not caused by the BL development. A possible
24 explanation might be that the photochemical production of ozone is enhanced at early noon
25 during summertime, leading to a delayed noontime minimum. The in-situ ozone
26 production/destruction in different seasons is not well quantified at the moment. Previous
27 studies focused on modelling the photochemical net production in winter and summer,
28 reporting net ozone production in winter and destruction in summer (Ma et al., 2002b).
29 Observation results, however, suggest that there should be net photochemical production
30 during summertime (Wang et al., 2006b). Hence there is a need for more investigation into
31 the cause for such a phenomenon.

1

2 **3.2 Season-annual variation characteristics of ozone**

3 Fig. 4 displays the season-annual variation of surface ozone during 1994-2013. Again, the
4 ozone mixing ratios peak in summer and are lowest during winter (Fig. 4b), with an average
5 seasonal peak occurring in June during 1994-2013 (Fig. 4c). Previous studies reported the
6 same seasonal ozone pattern, but attributed the summertime peak to different causes, e.g.,
7 more frequent STE events (Ding and Wang, 2006; Tang et al., 2011), enhanced vertical
8 convection (Ma et al., 2005), long-range transport from eastern-central China, central-
9 southern Asia or even Europe during summer (Zhu et al., 2004) and stronger cross boundary
10 transport and vertical convection during the East Asian summer monsoon season (Yang et al.,
11 2014). From Fig. 2c it can be noted that nighttime subsiding wind is indeed strongest in
12 summer, which supports the hypothesis of downward transport of ozone. Zheng et al. (2011)
13 argued that STE reaches maximum strength in spring and shows a decline in late spring based
14 on $^{10}\text{Be}/^7\text{Be}$ measurements, indicating that the continuous ozone increase in summer is caused
15 by the photochemical production.

16 The long-term variation of the annual average ozone exhibits a clear increasing trend (Fig. 4a).
17 A 2-4 year cycle seems to exist within the long-term variation of surface ozone. Previous
18 study has shown that there is a quasi-biannual oscillation (QBO) within the total ozone
19 column density over the Tibetan Plateau, which is in antiphase with the QBO of the tropical
20 stratospheric winds, exhibiting a 29-month cycle (Ji et al., 2001). The influence of the QBO
21 could extend to WLG station at the 3.8 km altitude via STE. Thus, surface ozone at WLG
22 might also have a QBO with a similar periodicity, which is related to that of the total ozone
23 column. The periodicity within the surface ozone data will be further discussed in sect. 3.4.

24 **3.3 Long-term trends of ozone**

25 The trends of monthly average all-day, daytime and nighttime ozone during 1994-2013 are
26 displayed in Figs. 5a1-c1, respectively. Ozone data in Figs. 5b1 and 5c1 are the subsets of
27 data from the daytime and nighttime ranges determined in Section 2.2 based on the zonal
28 wind information. The increase in surface ozone in the past two decades is evident in all three
29 data subsets, with a slightly stronger increase in the nighttime data. The linear trends for all-
30 day, daytime and nighttime ozone mixing ratios reached 0.25 ± 0.17 , 0.24 ± 0.16 and

1 0.28±0.17 ppbv yr⁻¹, respectively, while the Theil-Sen trend estimates reached 0.18, 0.17,
2 0.19 ppbv yr⁻¹, respectively. The Theil-Sen trend estimate is smaller than the linear regression
3 slope, mainly because the linear regression method is influenced by the seasonality within the
4 data. However, both methods yielded statistically significant increasing trends.

5 To further investigate the trend of ozone in different seasons, the trend of seasonal average
6 ozone during 1994-2013 was calculated and are shown in Figs. 5a-c (2-5). After eliminating
7 the seasonality in the data, the linear least squares fitting slopes and Theil-Sen trend estimates
8 yielded very similar results, thus only the linear slopes and p-values are listed in Table 1. The
9 strongest increase in surface ozone is found in autumn (SON), followed by spring (MAM),
10 respectively reaching 0.28±0.11 and 0.24±0.11 ppbv yr⁻¹ in the seasonal average of all-day
11 ozone mixing ratios. In comparison, summer (JJA) and winter (DJF) both show much weaker
12 increasing trends, with rates of 0.15±0.19 and 0.14±0.09 ppbv yr⁻¹, respectively, and the
13 summertime trend cannot even reach a confidence level of 95%. In summer the daytime
14 increasing rate is significantly lower than the nighttime one, respectively reaching 0.07±0.18
15 and 0.22±0.20 ppbv yr⁻¹. The nighttime slope reaches the confidence level of 95%, while the
16 daytime slope is statistically insignificant.

17 Previous investigations on the air-mass origin of WLG have shown that WLG is mostly
18 governed by western and northwestern air-masses, air-masses coming from the eastern sector
19 takes up only 2%, 5% and 8% in winter, spring and autumn, respectively (Zhang et al., 2011).
20 However, a significant percentage (30%) of air-masses come from the eastern direction during
21 summertime. Since the two major cities in the vicinity of WLG are both in the east,
22 summertime is believed to be the season in which WLG is most influenced by nearby
23 anthropogenic activities. From the diurnal variation of the horizontal wind speeds (Figs. 2a-b)
24 it can be discerned that daytime winds are weak northerly winds, while nighttime winds are
25 rather strong north-easterly winds, which are more in favour of transporting anthropogenic
26 pollution to WLG.

27 As already mentioned before in Section 3.2, some researchers believe that STE is also most
28 frequent in summer at WLG (Ding and Wang, 2006). During the night the WLG site is
29 governed by downwards winds, which may bring down air with high ozone mixing ratios
30 from above. Hence, an increase in the frequency of STE events would also result in increasing
31 nighttime ozone mixing ratios in summer. Whether it is anthropogenic activities or rather

1 meteorological factors, that has led to the distinct daytime and nighttime ozone variation
2 slopes in summer, still needs further investigations.

3 The seasonal peak of ozone in the northern midlatitudes typically occurs in summer over
4 populated continental areas, due to local and regional photochemical production and in late
5 spring for remote continental areas, due to both enhanced stratospheric input and
6 photochemical production in that season (Monks, 2000; Parrish et al., 2013). Recently, a shift
7 in the seasonal peak towards an earlier time in year has been observed at several high
8 elevation sites (Cooper et al., 2014; Parrish et al., 2013). Unlike other remote sites in the
9 northern midlatitudes, the seasonal ozone peak at WLG occurs in summer. However, the
10 largest increase in ozone mixing ratio is found in autumn rather than in summer. Lin et al.
11 (2014) also reported significant increasing ozone trends in autumn rather than spring at the
12 Mauna Loa Observatory in Hawaii in the past 4 decades and attributed this phenomenon to
13 strengthened ozone-rich air mass transport from Eurasia. The fact that we observed the largest
14 ozone increase in autumn is possibly linked to changes in atmospheric circulation. Details will
15 be discussed in the companion paper.

16 Here we present a comparison of our ozone trends in different seasons with those at other
17 high altitude (>1200 m asl) sites in the northern hemisphere, which have been reported in
18 literature and are based on time ranges similar to that of WLG (Table 2). The stations have
19 been sorted by latitude. The low latitude sites, Mauna Loa and Izaña, both show increasing
20 trends (0.31 ± 0.07 and 0.14 ± 0.05 ppbv yr⁻¹) during 1991-2010 (Oltmans et al., 2013). Lin et al.
21 (2014) compared the ozone levels at the Mauna Loa site in Hawaii during the period of 1995
22 to 2011 to that of 1980 to 1995, and discovered a strong increase during summer and autumn.
23 The mid-latitude stations exhibit inconsistent trends. Significantly positive trends were
24 detected at Mt. Happo, Japan (0.65 ± 0.32 ppbv yr⁻¹, Cooper et al., 2014), at the Rocky
25 Mountains National Park site, USA (0.33 ± 0.05 ppbv yr⁻¹, Oltmans et al., 2013), at Lassen
26 Volcanic National Park, USA (0.27 ± 0.13 ppbv yr⁻¹, Cooper et al., 2014) and at Jungfraujoch,
27 Switzerland (0.32 ± 0.18 ppbv yr⁻¹, Cui et al., 2011). Tarasova et al. (2009) found evidence for
28 increased stratospheric contribution to surface ozone at Jungfraujoch. The strongest increase
29 at Jungfraujoch was detected in winter and the weakest in summer. Gilge et al. (2010) also
30 reported increased wintertime ozone at two other alpine sites in central Europe during 1995-
31 2007. Cooper et al. (2014) reported significant daytime increasing trends at Lassen Volcanic
32 National Park during spring (0.39 ± 0.15 ppbv yr⁻¹) and winter (0.21 ± 0.14 ppbv yr⁻¹). Lin et al.

1 (2015b) reported an increasing trend of 0.31 ± 0.21 ppbv yr⁻¹ in springtime free-tropospheric
2 ozone over western North America during 1995-2014, however, by shutting off North
3 American emissions in the model and focusing on the subset of ozone associated with Asian
4 influence (also possibly mixed with stratospheric intrusions), the baseline ozone revealed a
5 more significant increasing rate of 0.55 ± 0.14 ppbv yr⁻¹ during 1992-2012. No significant
6 trends were found at Gothic, USA, Pinadale, USA and Zugspitze, Germany. Negative trends
7 were revealed at Kislovodsk, Russia (-0.37 ± 0.14 ppbv yr⁻¹, Tarasova et al., 2009) and the
8 Whiteface Mountain Summit site, USA (-0.22 ± 0.06 ppbv yr⁻¹, Oltmans, 2013). Tarasova et al.
9 (2009) attributed the strong decrease in ozone at Kislovodsk to control measures of Europe
10 and the breakdown of the former USSR. Both the strong increasing and decreasing trends at
11 Jungfraujoch and Kislovodsk were mostly caused by the variation in ozone mixing ratios in
12 the 1990s. The positive trend at Jungfraujoch during the 1990s was strongest in spring and
13 weakest in summer and autumn, while the reduction at Kislovodsk was strongest in summer
14 and weaker in autumn and winter (Tarasova et al., 2009). After 2000, the eastern U.S. was
15 revealed significant decrease due to the implementation of NO_x emission control measures,
16 while ozone mixing ratios at the other sites in the northern mid-latitudes have entered a steady
17 stage with either slow or no growth (Tarasova et al., 2009; Oltmans et al., 2013).

18 In comparison, WLG shows a continuous rise of ozone mixing ratio throughout the past two
19 decades and the most significant positive trends appear in autumn and spring, unlike the other
20 mid-latitude stations.

21 **3.4 Hilbert-Huang Spectral Analysis of surface ozone at WLG**

22 The long-term variation of surface ozone may be the result of changes in emissions of ozone
23 precursors, but may also be caused by year-to-year fluctuations or multiyear oscillations of
24 climate conditions. All the related factors have different periodicities, which cause the non-
25 linear variations of ozone. To unravel the potential oscillations on different time scales in the
26 ozone timeseries, we performed an HHT analysis on the ozone data from WLG using the
27 method described in Section 2.4. Our effort is the first time that the HHT method has been
28 applied in the analysis of atmospheric composition data. The first step of this analysis was the
29 EMD filtering of the timeseries of monthly average ozone mixing ratio. The results of the
30 EMD are shown in Fig. 6. The monthly average ozone signal could be decomposed into 5
31 IMFs with different characteristic time scales. The lowest order IMF (c1) shows an oscillation
32 with the highest frequency. The second IMF (c2) shows the seasonal variation in the ozone

1 signal. C3 reveals 3-4 year oscillations, c4 shows 7 year oscillations and the highest order
2 IMF (c5 in Fig. 6f) shows the longest oscillations pattern, with a quasi-11-year periodicity.

3 A segmentation analysis was performed by finding the local extrema of c5. The total time
4 span can be separated into 4 segments, as indicated by the dotted lines in Fig. 6a. The slopes
5 of the segments of c5 indicate whether the value is increasing or declining. To determine the
6 significance of the trend, the modified Mann-Kendall trend test was performed on each
7 segment and the results are given in Table 3. The first segment lasted 3 years (from Aug.
8 1994 to Jun. 1997) and revealed no significant trend ($z=1.42$), with an increasing slope of
9 $0.27 \text{ ppbv yr}^{-1}$. The second segment lasted for 5 years (from Jul. 1997 to May 2002) and
10 displayed a significant upward trend ($z=3.66$), with an increasing slope of $0.42 \text{ ppbv yr}^{-1}$.
11 Afterwards the increase of the ozone mixing ratio at WLG slowed down in segment 3, lasting
12 6 years (from Jun. 2002 to Apr. 2008), with an increasing slope of $0.30 \text{ ppbv yr}^{-1}$, however,
13 the increasing trend remained significant ($z=3.57$). In the last segment (from May 2008 to the
14 end of Jul. 2013), the significant upward trend continued ($z=3.65$) with a larger increasing
15 slope ($0.36 \text{ ppbv yr}^{-1}$) than that in segment 3.

16 Overall, surface ozone mixing ratio at WLG increased continuously from 1997 to 2013. Fig.
17 7a shows the anomaly of the interpolated monthly average ozone during 1994-2013, its
18 overall trend (represented by $c5+r$ in Fig. 6) and its variation on a scale of 7-year or longer
19 (represented by $c4+c5+r$ in Fig. 6). The corresponding variation slopes of the overall trend
20 and the 7-year or longer variation are depicted in Fig. 7b. The overall trend confirms the
21 continuous increase since Jan. 1997. The two largest slopes are respectively detected in May
22 2000 and Oct. 2010. The 7-year or longer trend line displays a rise in ozone after Aug. 1996,
23 which reaches a maximum increasing speed in Sep. 2003. Afterwards, the increase slows
24 down and turns into a decreasing trend in Sep. 2005. After Jan. 2009, ozone mixing ratios
25 went up again, reaching a maximum increasing speed in Dec. 2010.

26 The Hilbert Energy Spectrum is depicted in Fig. 8d, along with the volatility, instantaneous
27 energy (IE) and the degree of stationarity (DS) (Figs. 8b, 8c and 8e). Both the volatility and
28 the IE reflect the variation of energy with time. Compared to the mean IE, which represents
29 the temporal variation of the frequency averaged energy, volatility rather focuses on the ratio
30 of the variation of certain signals to the total signal. Peaks in the mean IE can be found in
31 1994-1995, 2000-2001, 2003, 2008 and 2013 (Fig. 8c), which correspond to the high ozone
32 mixing ratio values in the data. High values of volatility are found around 2003, 2008 and

1 2012 (Fig. 8b), which mostly agree with those of the IE. The cause for these high anomalies
2 still needs to be investigated.

3 The DS corresponding to each frequency, as displayed in Fig. 8e, can provide information on
4 the underlying periodicity within the original signal. The smaller the DS is, the more
5 stationary the data is at this frequency. Lower DS values are observed in the low frequency
6 part. A local minimum at the frequencies between 0.08 and 0.12 can be found, which
7 corresponds to the annual cycle of ozone. Other local minima are found at even lower
8 frequencies, corresponding to 2.5a, 3.5a, 7a and 11a cycles. Among all the known
9 atmospheric factors that have an impact on the ozone mixing ratio at WLG, QBO, ENSO, etc.,
10 could be responsible for these periodicities.

11 Overall, the HHT analysis is able to detect variations in surface ozone trends during different
12 periods, and is successful in finding the anomalies and periodicities within the data. Results of
13 this analysis can further facilitate the attribution of the variations of surface ozone at WLG to
14 the influencing factors, which will be discussed in the companion paper.

15 **4 Summary**

16 In this paper we present the characteristics, trends and periodicity of surface ozone mixing
17 ratio at a global baseline GAW station in the eastern Tibetan Plateau region (Mt. Waliguan)
18 during the past two decades. The trends and periodicity of ozone are investigated using a
19 modified Mann-Kendall test and an adaptive method (Hilbert Huang Transform) that is suited
20 for analysing non-stationary and non-linear natural processes.

21 While confirming the reported diurnal and seasonal characteristics of surface ozone at WLG,
22 our study reveals a relationship between the seasonality in mountain-valley breeze and the
23 seasonal shift in the occurrence time of daily maximum and minimum ozone at the site. Based
24 on this relationship, season-dependent daytime and nighttime periods are defined for
25 separately analysing the daytime and nighttime trends of surface ozone. Both daytime and
26 nighttime surface ozone have increased significantly at WLG. Autumn and spring revealed
27 the largest increase rates, while summer and winter showed relatively weaker increases. A
28 significant daytime and nighttime difference in trend could only be found in summer, where
29 nighttime ozone was significantly increasing and daytime ozone had no significant trend.
30 Results of the HHT spectral analysis confirm the increasing trends in surface ozone mixing
31 ratio and further identify four different stages with different increasing rates. The overall trend
32 indicates that the largest increase occurred around May 2000 and Oct. 2010. The ozone signal

1 can be decomposed into five intrinsic mode functions with different time scales. 2-4 year, 7
2 year and 11 year periodicities are found within the data, the cause of which still needs further
3 investigation.

4 The results obtained in this work are valuable for related climate and environment change
5 assessments of western China and surrounding areas, and can be used in the validation of
6 chemistry-climate models. As WLG is a high altitude mountain-top site in a remote region,
7 measurements of surface ozone and other species can well represent a large scale situation.
8 Previous air mass origin and modelling studies (Zhang et al., 2011; Li et al., 2014) suggest that
9 WLG is mostly under the influence of transport from the north-west direction, hence the
10 upward trend in ozone might be an indication of impact of transport from that direction. Since
11 eastern China is downwind of WLG, our results imply that under rising baseline ozone
12 conditions, even greater effort needs to be applied to reducing ozone precursors in eastern
13 China in order to improve ozone air quality. In the second part of our study, influencing
14 factors or potential causes of the observed long-term trends of surface ozone at WLG will be
15 addressed and discussed.

17 **Data availability**

18 The ozone data analyzed in this work are partly available at the World Data Center for
19 Greenhouse Gases (WDCGG) ([http://ds.data.jma.go.jp/gmd/wdcgg/cgi-bin/wdcgg](http://ds.data.jma.go.jp/gmd/wdcgg/cgi-bin/wdcgg/download.cgi?index=WLG236N00-CMA¶m=201405120001&select=inventory)
20 [/download.cgi?index=WLG236N00-CMA¶m=201405120001&select=inventory](http://ds.data.jma.go.jp/gmd/wdcgg/cgi-bin/wdcgg/download.cgi?index=WLG236N00-CMA¶m=201405120001&select=inventory)). The
21 entire dataset can be made available for scientific purposes upon request to the authors.

23 **Acknowledgements**

24 We thank all operators of the Mt. Waliguan Baseline Station for their excellent routine work.
25 We appreciate WMO/GEF, WMO/GAW, Canada/AES, and Swiss/WCC-Empa for funding
26 and technical support. This work is supported by China Special Fund for Meteorological
27 Research in the Public Interest (No. GYHY201106023), Environmental Protection Public
28 Welfare Scientific Research Project, Ministry of Environmental Protection of the People's
29 Republic of China (Grant No. 201509002), the Natural Science Foundation of China (No.
30 41505107 and 21177157) and the Basic Research Fund of CAMS (No. 2013Z005).

1 **References**

- 2 Ambrose, J. L., Reidmiller, D. R., and Jaffe, D. A.: Causes of high O₃ in the lower free
3 troposphere over the Pacific Northwest as observed at the Mt. Bachelor Observatory,
4 Atmospheric Environment, 45, 5302-5315, <http://dx.doi.org/10.1016/j.atmosenv.2011.06.056>,
5 2011.
- 6 Cooper, O. R., Parrish, D. D., Stohl, A., Trainer, M., Nedelec, P., Thouret, V., Cammas, J. P.,
7 Oltmans, S. J., Johnson, B. J., Tarasick, D., Leblanc, T., McDermid, I. S., Jaffe, D., Gao, R.,
8 Stith, J., Ryerson, T., Aikin, K., Campos, T., Weinheimer, A., and Avery, M. A.: Increasing
9 springtime ozone mixing ratios in the free troposphere over western North America, *Nature*,
10 463, 344-348, 10.1038/nature08708, 2010.
- 11 Cooper, O. R., Parrish, D., Ziemke, J., Balashov, N., Cupeiro, M., Galbally, I., Gilge, S.,
12 Horowitz, L., Jensen, N., and Lamarque, J.-F.: Global distribution and trends of tropospheric
13 ozone: An observation-based review, *Elementa: Science of the Anthropocene*, 2, 000029,
14 2014.
- 15 Cui, J., Pandey Deolal, S., Sprenger, M., Henne, S., Staehelin, J., Steinbacher, M., and
16 Nédélec, P.: Free tropospheric ozone changes over Europe as observed at Jungfraujoch
17 (1990–2008): An analysis based on backward trajectories, *Journal of Geophysical Research:*
18 *Atmospheres*, 116, n/a-n/a, 10.1029/2010JD015154, 2011.
- 19 Ding, A., and Wang, T.: Influence of stratosphere-to-troposphere exchange on the seasonal
20 cycle of surface ozone at Mount Waliguan in western China, *Geophysical Research Letters*,
21 33, L03803, 10.1029/2005GL024760, 2006.
- 22 Ding, A. J., Wang, T., Thouret, V., Cammas, J. P., and Nédélec, P.: Tropospheric ozone
23 climatology over Beijing: analysis of aircraft data from the MOZAIC program, *Atmos. Chem.*
24 *Phys.*, 8, 1-13, 10.5194/acp-8-1-2008, 2008.
- 25 El-Askary, H., Sarkar, S., Chiu, L., Kafatos, M., and El-Ghazawi, T.: Rain gauge derived
26 precipitation variability over Virginia and its relation with the El Nino southern oscillation,
27 *Advances in Space Research*, 33, 338-342, [http://dx.doi.org/10.1016/S0273-1177\(03\)00478-2](http://dx.doi.org/10.1016/S0273-1177(03)00478-2),
28 2004.
- 29 Gilge, S., Plass-Duelmer, C., Fricke, W., Kaiser, A., Ries, L., Buchmann, B., and Steinbacher,
30 M.: Ozone, carbon monoxide and nitrogen oxides time series at four alpine GAW mountain
31 stations in central Europe, *Atmos. Chem. Phys.*, 10, 12295-12316, 10.5194/acp-10-12295-
32 2010, 2010.
- 33 Hamed, K. H., and Ramachandra Rao, A.: A modified Mann-Kendall trend test for
34 autocorrelated data, *Journal of Hydrology*, 204, 182-196, [http://dx.doi.org/10.1016/S0022-
35 1694\(97\)00125-X](http://dx.doi.org/10.1016/S0022-1694(97)00125-X), 1998.
- 36 Helsel, D. R., Mueller, D. K., and Slack, J. R.: Computer program for the Kendall family of
37 trend tests: U.S. Geological Survey Scientific Investigations Report 2005-5275, 4p.b,
38 <http://pubs.usgs.gov/sir/2005/5275/pdf/sir2005-5275.pdf>, 2006.
- 39 Huang, N. E., Shen, Z., Long, S. R., Wu, M. C., Shih, H. H., Zheng, Q., Yen, N.-C., Tung, C.
40 C., and Liu, H. H.: The empirical mode decomposition and the Hilbert spectrum for nonlinear
41 and non-stationary time series analysis, *Proceedings of the Royal Society of London A:*
42 *Mathematical, Physical and Engineering Sciences*, 1998, 903-995,

- 1 Huang, N. E., Wu, M.-L. C., Long, S. R., Shen, S. S., Qu, W., Gloersen, P., and Fan, K. L.: A
2 confidence limit for the empirical mode decomposition and Hilbert spectral analysis,
3 Proceedings of the Royal Society of London A: Mathematical, Physical and Engineering
4 Sciences, 2003, 2317-2345,
- 5 Huang, N. E., and Wu, Z.: A review on Hilbert-Huang transform: Method and its applications
6 to geophysical studies, Reviews of Geophysics, 46, RG2006, 10.1029/2007RG000228, 2008.
- 7 Huang, N. E.: Hilbert-Huang transform and its applications, World Scientific, 2014.
- 8 IPCC: Climate Change 2013: The Physical Science Basis. Contribution of Working Group I
9 to the Fifth Assessment Report of the Intergovernmental Panel on Climate Change,
10 Cambridge Univ. Press, Cambridge, United Kingdom and New York, NY, USA, 1535, 2013.
- 11 Ji, C. P., Zou, H., and Zhou, L. B.: QBO Signal in Total Ozone Over the Tibet, Climatic and
12 Environmental Research, 6, 416-424, 2001.
- 13 Jia, S., Xu, X., Lin, W., Wang, Y., He, X., and Zhang, H.: Increased mixing ratio of surface
14 ozone by nighttime convection process over the North China Plain, Journal of Applied
15 Meteorological Science, 26, 280-290, 2015.
- 16 Kendall, M. G.: Rank Correlation Methods, Charles Griffin, London, 1955.
- 17 Lal, S., Venkataramani, S., Chandra, N., Cooper, O. R., Brioude, J., and Naja, M.: Transport
18 effects on the vertical distribution of tropospheric ozone over western India, Journal of
19 Geophysical Research: Atmospheres, 2014JD021854, 10.1002/2014JD021854, 2014.
- 20 Langford, A. O., Senff, C. J., Alvarez Ii, R. J., Brioude, J., Cooper, O. R., Holloway, J. S., Lin,
21 M. Y., Marchbanks, R. D., Pierce, R. B., Sandberg, S. P., Weickmann, A. M., and Williams,
22 E. J.: An overview of the 2013 Las Vegas Ozone Study (LVOS): Impact of stratospheric
23 intrusions and long-range transport on surface air quality, Atmospheric Environment, 109,
24 305-322, <http://dx.doi.org/10.1016/j.atmosenv.2014.08.040>, 2015.
- 25 Lefohn, A. S., Wernli, H., Shadwick, D., Oltmans, S. J., and Shapiro, M.: Quantifying the
26 importance of stratospheric-tropospheric transport on surface ozone concentrations at high-
27 and low-elevation monitoring sites in the United States, Atmospheric Environment, 62, 646-
28 656, <http://dx.doi.org/10.1016/j.atmosenv.2012.09.004>, 2012.
- 29 Lelieveld, J., and Dentener, F. J.: What controls tropospheric ozone?, Journal of Geophysical
30 Research: Atmospheres, 105, 3531-3551, 10.1029/1999JD901011, 2000.
- 31 Levy, H.: Normal Atmosphere: Large Radical and Formaldehyde Concentrations Predicted,
32 Science, 173, 141-143, 10.1126/science.173.3992.141, 1971.
- 33 Li, X., Liu, J., Mauzerall, D. L., Emmons, L. K., Walters, S., Horowitz, L. W., and Tao, S.:
34 Effects of trans-Eurasian transport of air pollutants on surface ozone concentrations over
35 Western China, Journal of Geophysical Research: Atmospheres, 119, 12,338-312,354,
36 10.1002/2014JD021936, 2014.
- 37 Lin, M., Fiore, A. M., Horowitz, L. W., Cooper, O. R., Naik, V., Holloway, J., Johnson, B. J.,
38 Middlebrook, A. M., Oltmans, S. J., Pollack, I. B., Ryerson, T. B., Warner, J. X., Wiedinmyer,
39 C., Wilson, J., and Wyman, B.: Transport of Asian ozone pollution into surface air over the
40 western United States in spring, Journal of Geophysical Research: Atmospheres, 117, n/a-n/a,
41 10.1029/2011JD016961, 2012.

- 1 Lin, M., Horowitz, L. W., Oltmans, S. J., Fiore, A. M., and Fan, S.: Tropospheric ozone
2 trends at Mauna Loa Observatory tied to decadal climate variability, *Nature Geosci*, 7, 136-
3 143, 10.1038/ngeo2066, 2014.
- 4 Lin, M., Fiore, A. M., Horowitz, L. W., Langford, A. O., Oltmans, S. J., Tarasick, D., and
5 Rieder, H. E.: Climate variability modulates western US ozone air quality in spring via deep
6 stratospheric intrusions, *Nat Commun*, 6, 10.1038/ncomms8105, 2015a.
- 7 Lin, M., Horowitz, L. W., Cooper, O. R., Tarasick, D., Conley, S., Iraci, L. T., Johnson, B.,
8 Leblanc, T., Petropavlovskikh, I., and Yates, E. L.: Revisiting the evidence of increasing
9 springtime ozone mixing ratios in the free troposphere over western North America,
10 *Geophysical Research Letters*, n/a-n/a, 10.1002/2015GL065311, 2015b.
- 11 Logan, J. A., Staehelin, J., Megretskaya, I. A., Cammas, J. P., Thouret, V., Claude, H., De
12 Backer, H., Steinbacher, M., Scheel, H. E., Stübi, R., Fröhlich, M., and Derwent, R.: Changes
13 in ozone over Europe: Analysis of ozone measurements from sondes, regular aircraft
14 (MOZAIC) and alpine surface sites, *Journal of Geophysical Research: Atmospheres*, 117,
15 D09301, 10.1029/2011JD016952, 2012.
- 16 Lundquist, J. K.: Intermittent and Elliptical Inertial Oscillations in the Atmospheric Boundary
17 Layer, *Journal of the Atmospheric Sciences*, 60, 2661-2673, 10.1175/1520-
18 0469(2003)060<2661:IAEIOI>2.0.CO;2, 2003.
- 19 Ma, J., Liu, H., and Hauglustaine, D.: Summertime tropospheric ozone over China simulated
20 with a regional chemical transport model 1. Model description and evaluation, *Journal of*
21 *Geophysical Research: Atmospheres*, 107, ACH 27-21-ACH 27-13, 10.1029/2001JD001354,
22 2002a.
- 23 Ma, J., Tang, J., Zhou, X., and Zhang, X.: Estimates of the Chemical Budget for Ozone at
24 Waliguan Observatory, *Journal of Atmospheric Chemistry*, 41, 21-48,
25 10.1023/A:1013892308983, 2002b.
- 26 Ma, J., Zheng, X., and Xu, X.: Comment on “Why does surface ozone peak in summertime at
27 Waliguan?” by Bin Zhu et al, *Geophysical Research Letters*, 32, n/a-n/a,
28 10.1029/2004GL021683, 2005.
- 29 Ma, J., Lin, W. L., Zheng, X. D., Xu, X. B., Li, Z., and Yang, L. L.: Influence of air mass
30 downward transport on the variability of surface ozone at Xianggelila Regional Atmosphere
31 Background Station, southwest China, *Atmos. Chem. Phys.*, 14, 5311-5325, 10.5194/acp-14-
32 5311-2014, 2014.
- 33 Ma, Z., Xu, J., Quan, W., Zhang, Z., Lin, W., and Xu, X.: Significant increase of surface
34 ozone at a rural site, north of eastern China, *Atmos. Chem. Phys.*, 16, 3969-3977,
35 10.5194/acp-16-3969-2016, 2016.
- 36 Monks, P. S.: A review of the observations and origins of the spring ozone maximum,
37 *Atmospheric Environment*, 34, 3545-3561, [http://dx.doi.org/10.1016/S1352-2310\(00\)00129-1](http://dx.doi.org/10.1016/S1352-2310(00)00129-1),
38 2000.
- 39 Monks, P. S., Archibald, A. T., Colette, A., Cooper, O., Coyle, M., Derwent, R., Fowler, D.,
40 Granier, C., Law, K. S., Mills, G. E., Stevenson, D. S., Tarasova, O., Thouret, V., von
41 Schneidmesser, E., Sommariva, R., Wild, O., and Williams, M. L.: Tropospheric ozone and
42 its precursors from the urban to the global scale from air quality to short-lived climate forcer,
43 *Atmos. Chem. Phys.*, 15, 8889-8973, 10.5194/acp-15-8889-2015, 2015.

1 Oltmans, S. J., Lefohn, A. S., Harris, J. M., Galbally, I., Scheel, H. E., Bodeker, G., Brunke,
2 E., Claude, H., Tarasick, D., Johnson, B. J., Simmonds, P., Shadwick, D., Anlauf, K., Hayden,
3 K., Schmidlin, F., Fujimoto, T., Akagi, K., Meyer, C., Nichol, S., Davies, J., Redondas, A.,
4 and Cuevas, E.: Long-term changes in tropospheric ozone, *Atmospheric Environment*, 40,
5 3156-3173, <http://dx.doi.org/10.1016/j.atmosenv.2006.01.029>, 2006.

6 Oltmans, S. J., Lefohn, A. S., Shadwick, D., Harris, J. M., Scheel, H. E., Galbally, I., Tarasick,
7 D. W., Johnson, B. J., Brunke, E. G., Claude, H., Zeng, G., Nichol, S., Schmidlin, F., Davies,
8 J., Cuevas, E., Redondas, A., Naoe, H., Nakano, T., and Kawasato, T.: Recent tropospheric
9 ozone changes – A pattern dominated by slow or no growth, *Atmospheric Environment*, 67,
10 331-351, <http://dx.doi.org/10.1016/j.atmosenv.2012.10.057>, 2013.

11 Parrish, D. D., Law, K. S., Staehelin, J., Derwent, R., Cooper, O. R., Tanimoto, H., Volz-
12 Thomas, A., Gilge, S., Scheel, H. E., Steinbacher, M., and Chan, E.: Long-term changes in
13 lower tropospheric baseline ozone concentrations at northern mid-latitudes, *Atmos. Chem.*
14 *Phys.*, 12, 11485-11504, 10.5194/acp-12-11485-2012, 2012.

15 Parrish, D. D., Law, K. S., Staehelin, J., Derwent, R., Cooper, O. R., Tanimoto, H., Volz-
16 Thomas, A., Gilge, S., Scheel, H. E., Steinbacher, M., and Chan, E.: Lower tropospheric
17 ozone at northern midlatitudes: Changing seasonal cycle, *Geophysical Research Letters*, 40,
18 1631-1636, 10.1002/grl.50303, 2013.

19 Rao, A. R., and Hsu, E.-C.: *Hilbert-Huang Transform Analysis of Hydrological and*
20 *Environmental Time Series*, 1 ed., Water Science and Technology Library, 60, Springer
21 Netherlands, 2008.

22 Sen, P. K.: Estimates of the regression coefficient based on Kendall's tau, *Journal of the*
23 *American Statistical Association*, 63, 1379-1389, 1968.

24 Stohl, A., Bonasoni, P., Cristofanelli, P., Collins, W., Feichter, J., Frank, A., Forster, C.,
25 Gerasopoulos, E., Gäggeler, H., James, P., Kentarchos, T., Kromp-Kolb, H., Krüger, B., Land,
26 C., Meloan, J., Papayannis, A., Priller, A., Seibert, P., Sprenger, M., Roelofs, G. J., Scheel, H.
27 E., Schnabel, C., Siegmund, P., Tobler, L., Trickl, T., Wernli, H., Wirth, V., Zanis, P., and
28 Zerefos, C.: Stratosphere-troposphere exchange: A review, and what we have learned from
29 STACCATO, *Journal of Geophysical Research: Atmospheres*, 108, 8516,
30 10.1029/2002JD002490, 2003.

31 Tang, Q., Prather, M. J., and Hsu, J.: Stratosphere-troposphere exchange ozone flux related to
32 deep convection, *Geophys. Res. Lett.*, 38, L03806, 10.1029/2010gl046039, 2011.

33 Tarasova, O. A., Senik, I. A., Sosonkin, M. G., Cui, J., Staehelin, J., and Prévôt, A. S. H.:
34 Surface ozone at the Caucasian site Kislovodsk High Mountain Station and the Swiss Alpine
35 site Jungfraujoch: data analysis and trends (1990–2006), *Atmos. Chem. Phys.*, 9, 4157-4175,
36 10.5194/acp-9-4157-2009, 2009.

37 The Royal Society: Ground-level ozone in the 21st century: future trends, impacts and policy
38 implications, The Royal Society0854037136,
39 https://royalsociety.org/~media/Royal_Society_Content/policy/publications/2008/7925.pdf,
40 2008.

41 Vingarzan, R.: A review of surface ozone background levels and trends, *Atmospheric*
42 *Environment*, 38, 3431-3442, <http://dx.doi.org/10.1016/j.atmosenv.2004.03.030>, 2004.

43 Wang, Q. Y., Gao, R. S., Cao, J. J., Schwarz, J. P., Fahey, D. W., Shen, Z. X., Hu, T. F.,
44 Wang, P., Xu, X. B., and Huang, R. J.: Observations of high level of ozone at Qinghai Lake

1 basin in the northeastern Qinghai-Tibetan Plateau, western China, *Journal of Atmospheric*
2 *Chemistry*, 72, 19-26, 10.1007/s10874-015-9301-9, 2015.

3 Wang, T., Ding, A., Gao, J., and Wu, W. S.: Strong ozone production in urban plumes from
4 Beijing, China, *Geophys. Res. Lett.*, 33, L21806, 10.1029/2006gl027689, 2006a.

5 Wang, T., Wong, H. L. A., Tang, J., Ding, A., Wu, W. S., and Zhang, X. C.: On the origin of
6 surface ozone and reactive nitrogen observed at a remote mountain site in the northeastern
7 Qinghai-Tibetan Plateau, western China, *Journal of Geophysical Research: Atmospheres*, 111,
8 D08303, 10.1029/2005JD006527, 2006b.

9 Wang, T., Wei, X. L., Ding, A. J., Poon, C. N., Lam, K. S., Li, Y. S., Chan, L. Y., and Anson,
10 M.: Increasing surface ozone concentrations in the background atmosphere of Southern China,
11 1994–2007, *Atmos. Chem. Phys.*, 9, 6217-6227, 10.5194/acp-9-6217-2009, 2009.

12 Wang, Y., Konopka, P., Liu, Y., Chen, H., Müller, R., Plöger, F., Riese, M., Cai, Z., and Lü,
13 D.: Tropospheric ozone trend over Beijing from 2002–2010: ozonesonde measurements and
14 modeling analysis, *Atmos. Chem. Phys.*, 12, 8389-8399, 10.5194/acp-12-8389-2012, 2012.

15 Xu, X., Lin, W., Wang, T., Yan, P., Tang, J., Meng, Z., and Wang, Y.: Long-term trend of
16 surface ozone at a regional background station in eastern China 1991–2006: enhanced
17 variability, *Atmos. Chem. Phys.*, 8, 2595-2607, 10.5194/acp-8-2595-2008, 2008.

18 Xu, X., Tang, J., and Lin, W.: The trend and variability of surface ozone at the global GAW
19 station Mt. WALIGUAN, China, in: "Second Tropospheric Ozone Workshop Tropospheric
20 Ozone Changes: Observations, state of understanding and model performances",
21 WMO/GAW report, WMO, Geneva, 49–55, 2011.

22 Xue, L. K., Wang, T., Zhang, J. M., Zhang, X. C., Deliger, Poon, C. N., Ding, A. J., Zhou, X.
23 H., Wu, W. S., Tang, J., Zhang, Q. Z., and Wang, W. X.: Source of surface ozone and reactive
24 nitrogen speciation at Mount Waliguan in western China: New insights from the 2006
25 summer study, *J. Geophys. Res.*, 116, D07306, 10.1029/2010jd014735, 2011.

26 Yang, Y., Liao, H., and Li, J.: Impacts of the East Asian summer monsoon on interannual
27 variations of summertime surface-layer ozone concentrations over China, *Atmos. Chem.*
28 *Phys.*, 14, 6867-6879, 10.5194/acp-14-6867-2014, 2014.

29 Young, P. J., Archibald, A. T., Bowman, K. W., Lamarque, J. F., Naik, V., Stevenson, D. S.,
30 Tilmes, S., Voulgarakis, A., Wild, O., Bergmann, D., Cameron-Smith, P., Cionni, I., Collins,
31 W. J., Dalsøren, S. B., Doherty, R. M., Eyring, V., Faluvegi, G., Horowitz, L. W., Josse, B.,
32 Lee, Y. H., MacKenzie, I. A., Nagashima, T., Plummer, D. A., Righi, M., Rumbold, S. T.,
33 Skeie, R. B., Shindell, D. T., Strode, S. A., Sudo, K., Szopa, S., and Zeng, G.: Pre-industrial
34 to end 21st century projections of tropospheric ozone from the Atmospheric Chemistry and
35 Climate Model Intercomparison Project (ACCMIP), *Atmos. Chem. Phys.*, 13, 2063-2090,
36 10.5194/acp-13-2063-2013, 2013.

37 Zellweger, C., Hofer, P., and Buchmann, B.: System and Performance Audit of Surface
38 Ozone and Carbon Monoxide at the China GAW Baseline Observatory Waliguan Mountain,
39 WCC-Empa Report 00/3Rep., 46 pp, Empa, Dübendorf, Switzerland,
40 http://gaw.empa.ch/audits/WLG_2000.pdf, 2000.

41 Zellweger, C., Klausen, J., and Buchmann, B.: System and Performance Audit of Surface
42 Ozone Carbon Monoxide and Methane at the Global GAW Station Mt. Waliguan, China,
43 October 2004, WCC-Empa Report 04/3Rep., 52 pp, Empa, Dübendorf, Switzerland,
44 http://gaw.empa.ch/audits/WLG_2004.pdf, 2004.

- 1 Zellweger, C., Klausen, J., Buchmann, B., and Scheel, H.-E.: System and Performance Audit
2 of Surface Ozone, Carbon Monoxide, Methane and Nitrous Oxide at the GAW Global Station
3 Mt. Waliguan and the Chinese Academy of Meteorological Sciences (CAMS) China, June
4 2009, WCC-Empa Report 09/2Rep., 61 pp, Empa, Dübendorf, Switzerland,
5 https://www.wmo.int/pages/prog/arep/gaw/documents/WLG_2009.pdf, 2009.
- 6 Zhang, F., Zhou, L. X., Novelli, P. C., Worthy, D. E. J., Zellweger, C., Klausen, J., Ernst, M.,
7 Steinbacher, M., Cai, Y. X., Xu, L., Fang, S. X., and Yao, B.: Evaluation of in situ
8 measurements of atmospheric carbon monoxide at Mount Waliguan, China, *Atmos. Chem.*
9 *Phys.*, 11, 5195-5206, 10.5194/acp-11-5195-2011, 2011.
- 10 Zheng, X. D., Shen, C. D., Wan, G. J., Liu, K. X., Tang, J., and Xu, X. B.: $\sim(10)\text{Be}/\sim 7\text{Be}$
11 implies the contribution of stratosphere-troposphere transport to the winter-spring surface
12 O_3 variation observed on the Tibetan Plateau, *Chin. Sci. Bull.*, 56, 84-88, 2011.
- 13 Zhu, B., Akimoto, H., Wang, Z., Sudo, K., Tang, J., and Uno, I.: Why does surface ozone
14 peak in summertime at Waliguan?, *Geophysical Research Letters*, 31, L17104,
15 10.1029/2004GL020609, 2004.
- 16
17

1 Table 1 The linear slope, 95% confidence interval (in ppbv yr⁻¹) and the p-values (in
 2 parenthesis) of all-year and seasonal average surface ozone mixing ratio for the all-day data
 3 and for the daytime and nighttime data subsets during 1994-2013

Data subset	All year	MAM	JJA	SON	DJF
All-day	0.25±0.17 (<0.01)	0.24±0.11 (<0.01)	0.15±0.19 (0.12)	0.28±0.11 (<0.01)	0.14±0.09 (<0.01)
Day	0.24±0.16 (<0.01)	0.24±0.11 (<0.01)	0.07±0.18 (0.41)	0.27±0.10 (<0.01)	0.15±0.09 (<0.01)
Night	0.28±0.17 (<0.01)	0.24±0.12 (<0.01)	0.22±0.20 (0.04)	0.29±0.11 (<0.01)	0.13±0.10 (0.01)

4
5

1
2
3
4

Table 2 The linear slopes (in ppbv yr⁻¹) and the 95% confidence intervals of all-year and seasonal average surface ozone mixing ratio at WLG and other north hemispheric high altitude sites.

Station (Location)	Time Span	All-year	MAM	JJA	SON	DJF	Reference
Mauna Loa, USA (19.5N, 155.6W, 3397 m asl)	1991-2010	0.31±0.07					(Oltmans et al., 2013)
Izaña, Spain (28.3N, 16.5W, 2367 m asl)	1991-2010	0.14±0.05					(Oltmans et al., 2013)
Waliguan, China (36.3N, 100.9E, 3816 m asl)	1994-2013	0.25±0.17	0.24±0.11	0.15±0.19	0.28±0.11	0.14 ±0.09	This work
Mt. Hapoo, Japan (36.7N, 137.8E, 1850 m asl)	1991-2011 (All year) 1990-2011 (Seasonal)	0.65±0.32					(Cooper et al., 2014)
Gothic, USA 39.0N, 107.0W, 2915 m asl)	1990-2011		0.01±0.20*	-0.01±0.27*		-0.02±0.12*	(Cooper et al., 2014)
Rocky Mountain National Park, USA (40.3N, 105.6W, 2743 m asl)	1991-2010	0.33±0.05					(Oltmans et al., 2013)
Lassen Volcanic National Park, USA (40.5N, 121.6W, 1756 m asl)	1988-2010 (All year) 1990-2011 (Seasonal)	0.27±0.13	0.39±0.15*	0.22±0.28*		0.21±0.14*	(Cooper et al., 2014)
Pinadale, USA (42.9N, 109.8W, 2743 m asl)	1991-2010	-0.05±0.04					(Oltmans et al., 2013)
Kislovodsk, Russia (43.70N, 42.70E, 2070 m asl)	1991-2006	-0.37±0.14	-0.20±0.20	-0.14±0.24	-0.60±0.21	-0.30±0.25	(Tarasova et al., 2009)
Whiteface Mountain Summit, USA (44.4N, 73.9W, 1484 m asl)	1991-2010	-0.22±0.06	-0.02±0.32*	-0.48±0.18*		0.09±0.20	(Oltmans et al., 2013; Cooper et al., 2014)
Jungfrauoch, Switzerland (46.5N, 8.0E, 3580 m asl)	1990-2008	0.32±0.18	0.33±0.22	0.22±0.28	0.33±0.16	0.49±0.17	(Cui et al., 2011)
Zugspitze, Germany (47.4N, 11.0E, 2960 m asl)	1991-2010	0.05±0.04					(Oltmans et al., 2013)

* Daytime (11:00 – 16:59 local time) ozone trends

5
6

1

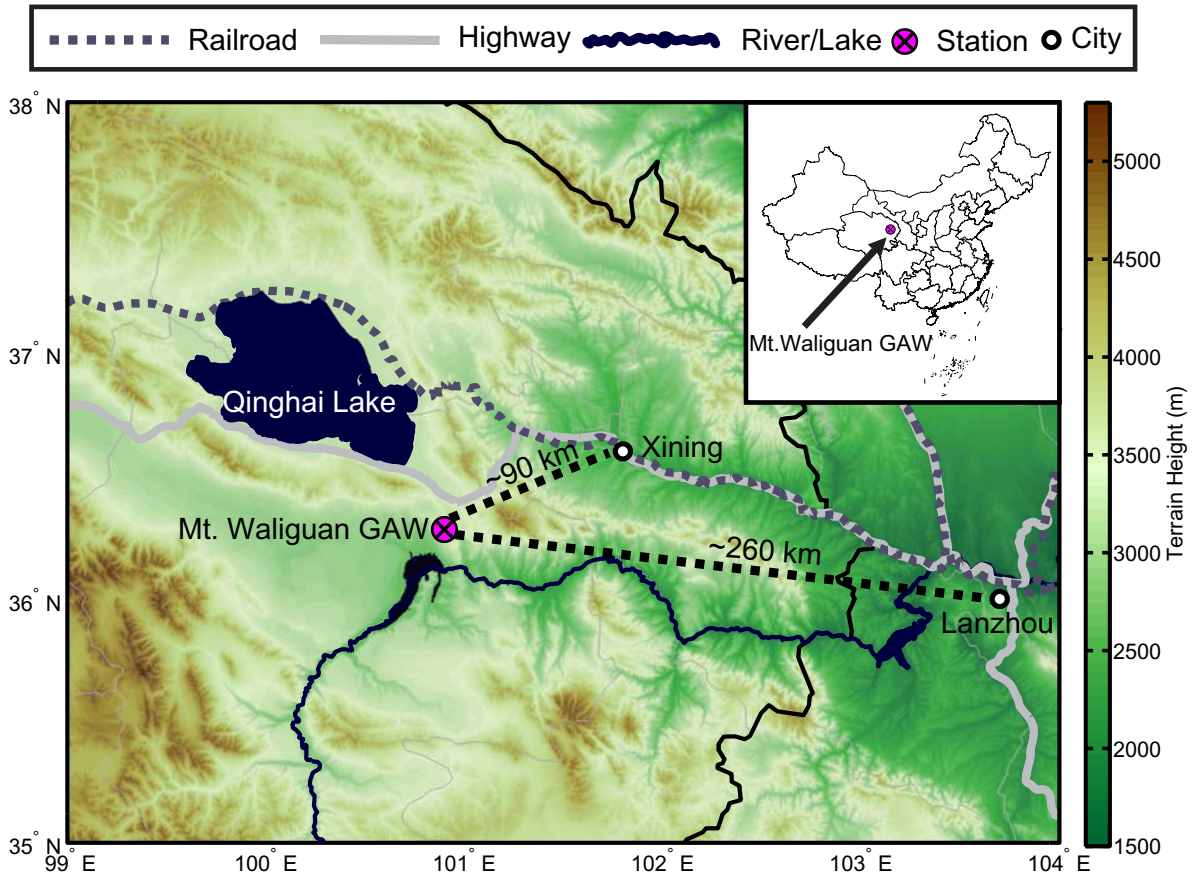
2 Table 3 Modified Mann-Kendall trend test on segments based on the last IMF.

Segment	Time Range	Slope of c5	Modified Mann-Kendall test (z)	Theil-Sen trend estimate of O ₃ (ppbv yr ⁻¹)
1	Aug.1994- Jun. 1997	-	No significant trend (z =1.42)	0.27
2	Jul. 1997-May 2002	+	Significant upward trend (z =3.66)	0.42
3	Jun. 2002-Apr. 2008	-	Significant upward trend (z =3.57)	0.30
4	May 2008-Jul. 2013	+	Significant upward trend (z = 3.42)	0.36

3

4

1

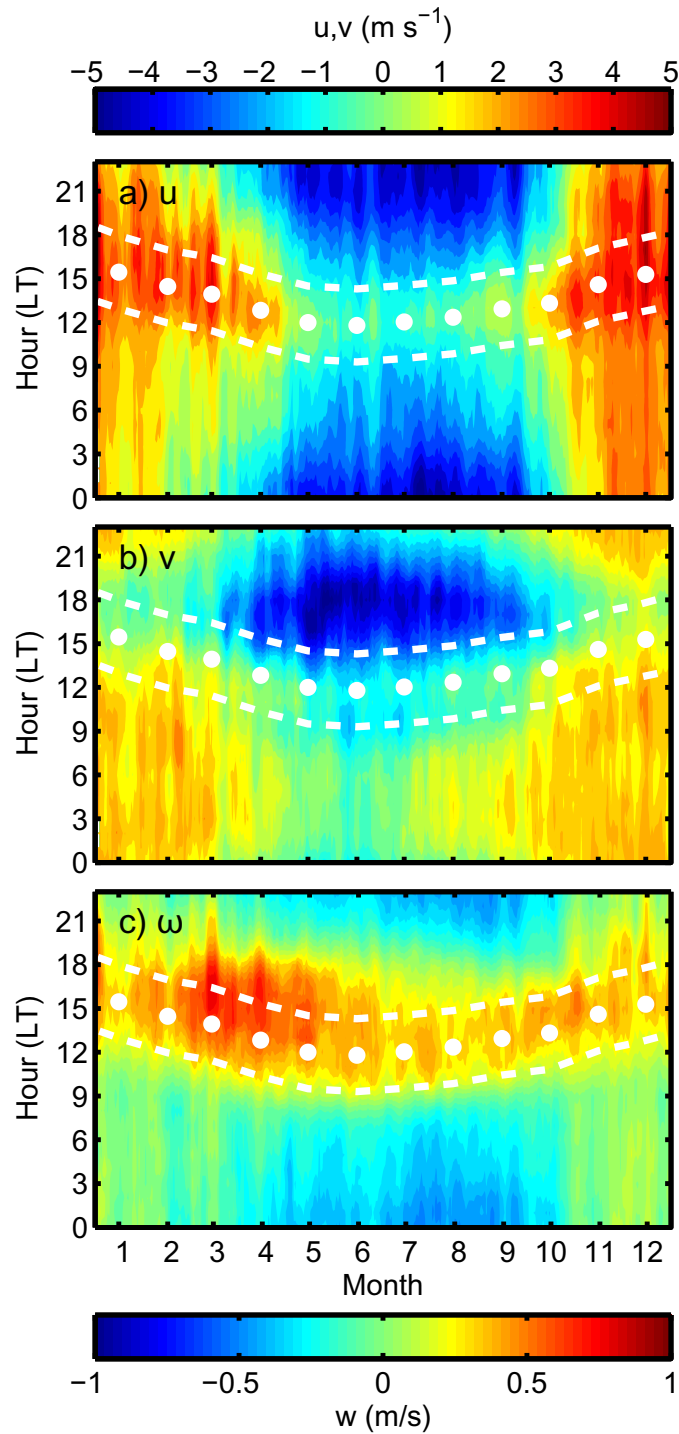


2

3 Figure 1 The location of the Mt. Waliguan GAW site and the two major cities in its vicinity.

4 The shading stands for the topographic height.

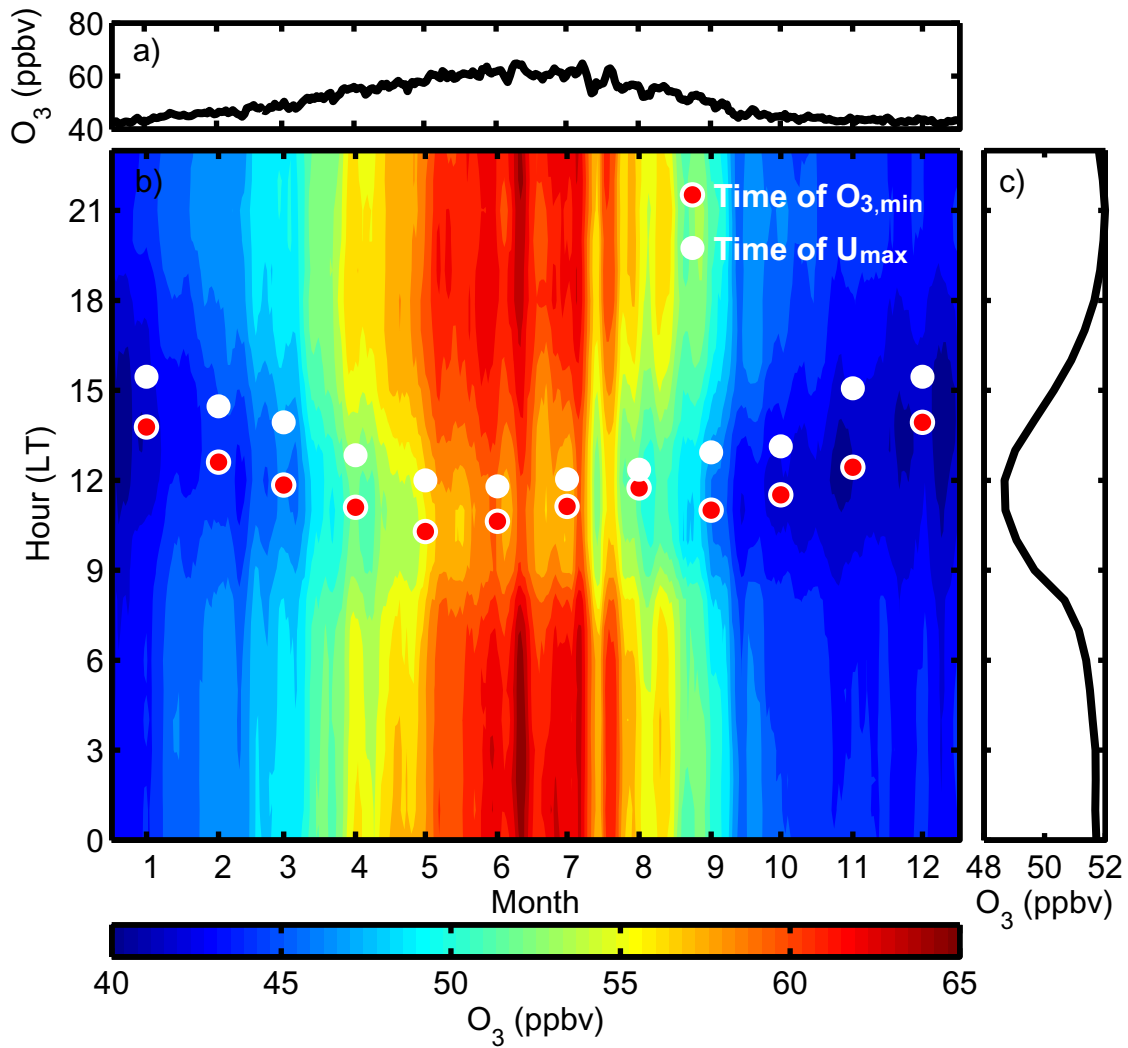
5



1

2 Figure 2 The average season-diurnal variation of surface zonal (a), meridional (b) and vertical
 3 (c) wind velocity on top of Mt. Waliguan during 1995-2013. The monthly average hour
 4 associated with the diurnal maximum zonal wind speed is given by the white dots, the
 5 daytime range is provided by the white dashed lines, which covers 6 hours centered around
 6 the white dots.

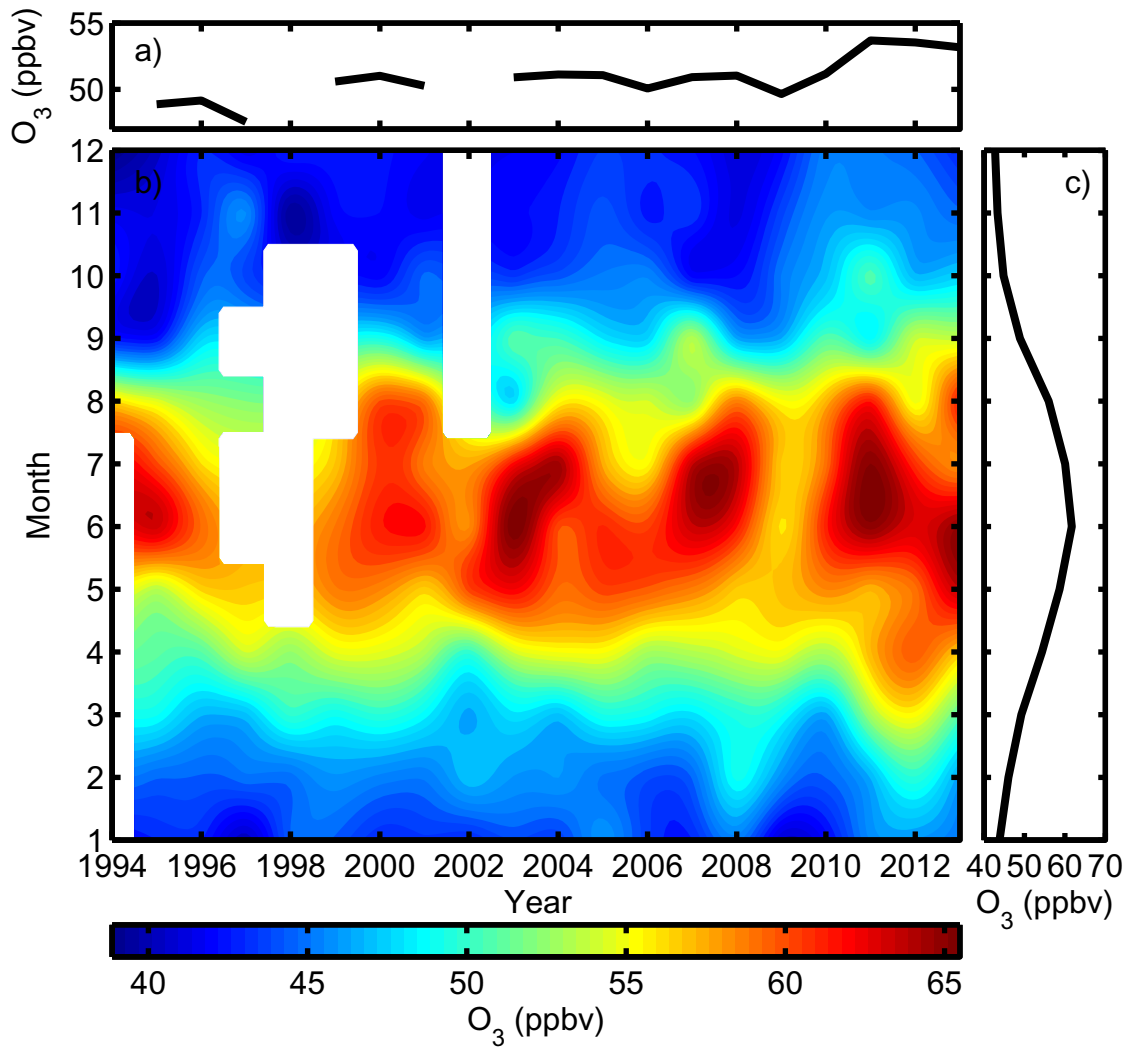
7



1

2 Figure 3 The average seasonal variation (a), season-diurnal variation (b) and diurnal variation
 3 (c) of ozone during 1995-2013. The red and white dots indicate the monthly average local
 4 times associated with the diurnal minimum ozone and the diurnal maximum zonal wind
 5 (U_{max}), respectively.

6

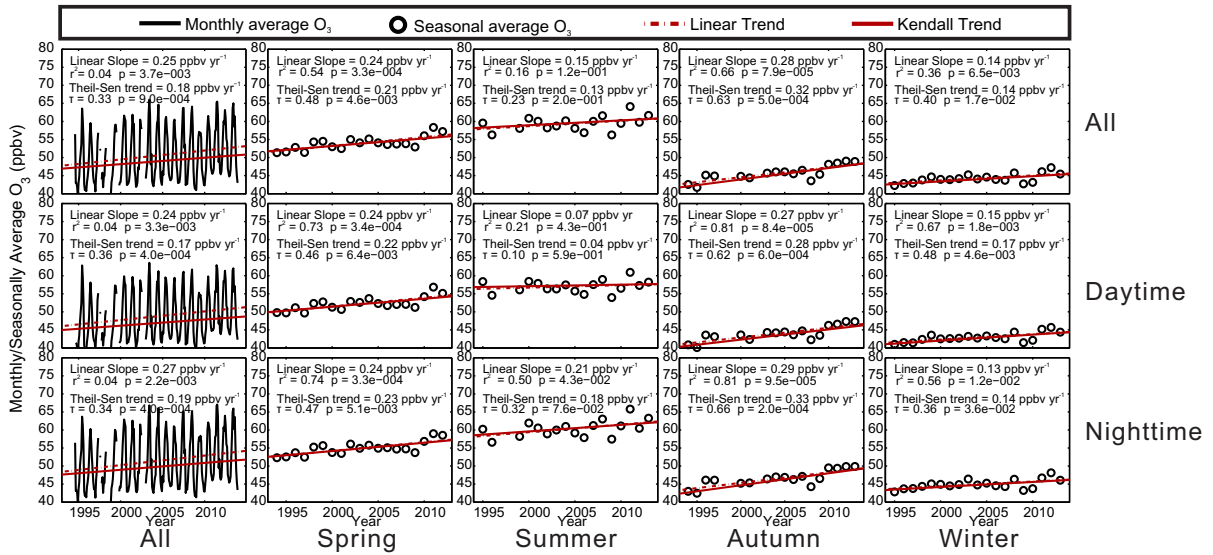


1

2 Figure 4 The average inter-annual variation (a), season-annual variation (b) and seasonal
 3 variation (c) of ozone during 1994-2013.

4

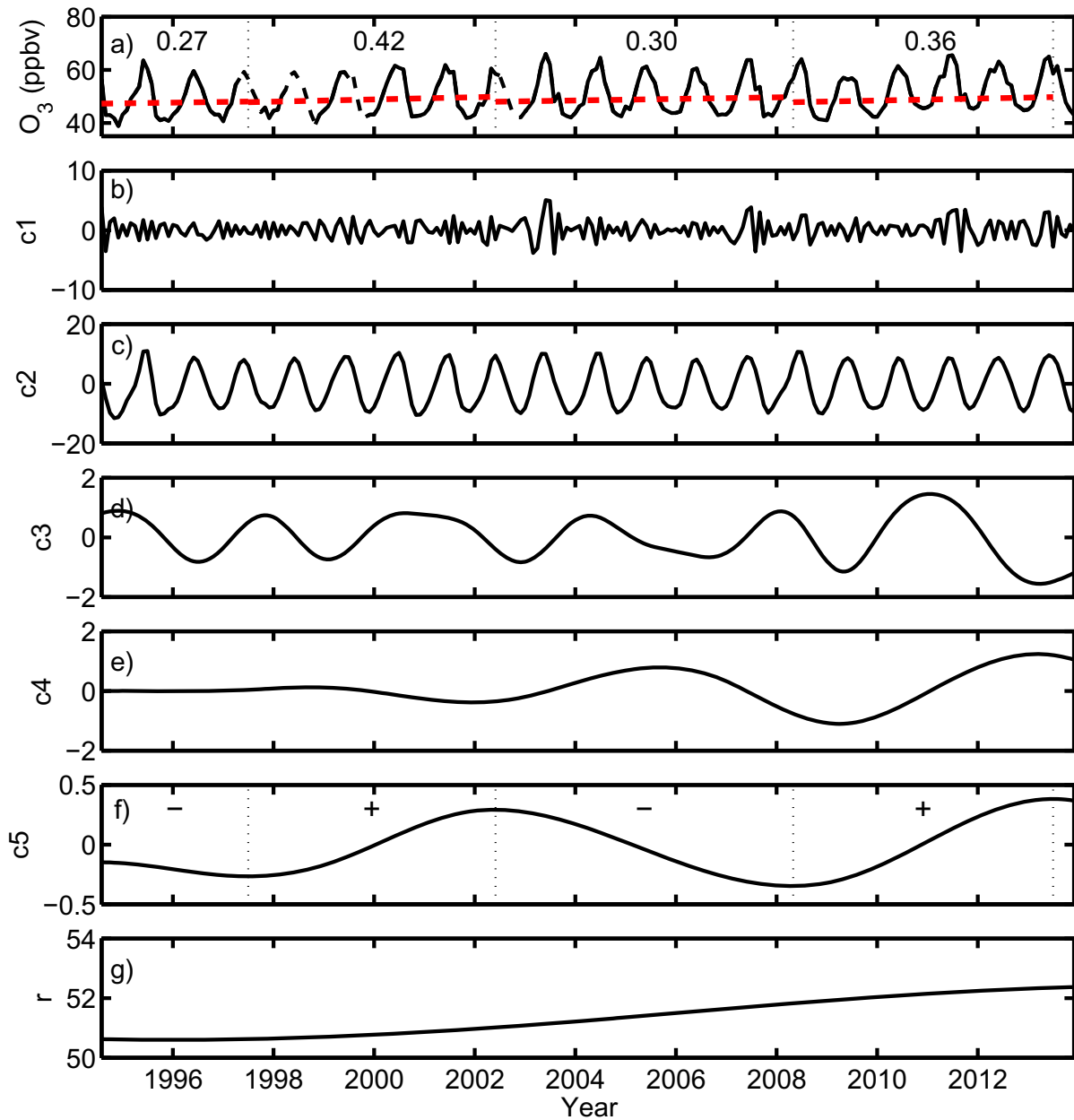
1



2

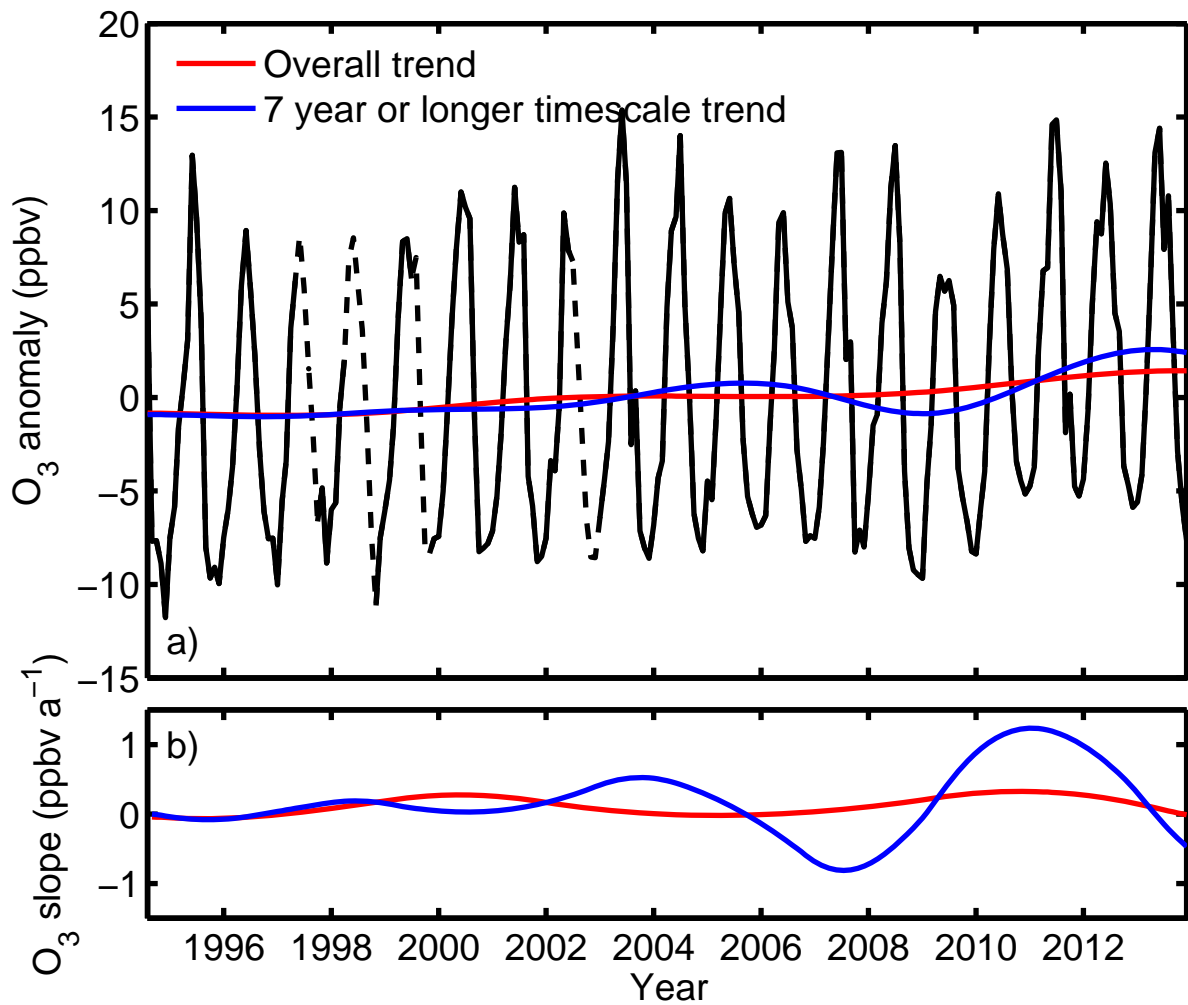
3 Figure 5 1) Monthly, 2) spring (MAM), 3) summer (JJA), 4) autumn (SON) and 5) winter
 4 time average all day (a), daytime (b) and nighttime (c) surface ozone mixing ratio during
 5 1994-2013 (black solid curves or black circles) and its trend (red lines: dotted line stands for
 6 the linear variation and solid line stands for the Theil-Sen trend estimates).

7



1
 2 Figure 6 The interpolated monthly average ozone mixing ratio at WLG from 1994 to 2013
 3 (the interpolated data given in dashed lines, a) and its intrinsic mode functions c_1 - c_5 (b-f,
 4 from the lowest to the highest order IMF) and its residue, r (g). The time segments in (a) were
 5 determined by the slope of the c_5 . The red slashed lines are the Theil-Sen trends and the
 6 numbers are the Theil-Sen trend estimates (in ppbv yr^{-1}).

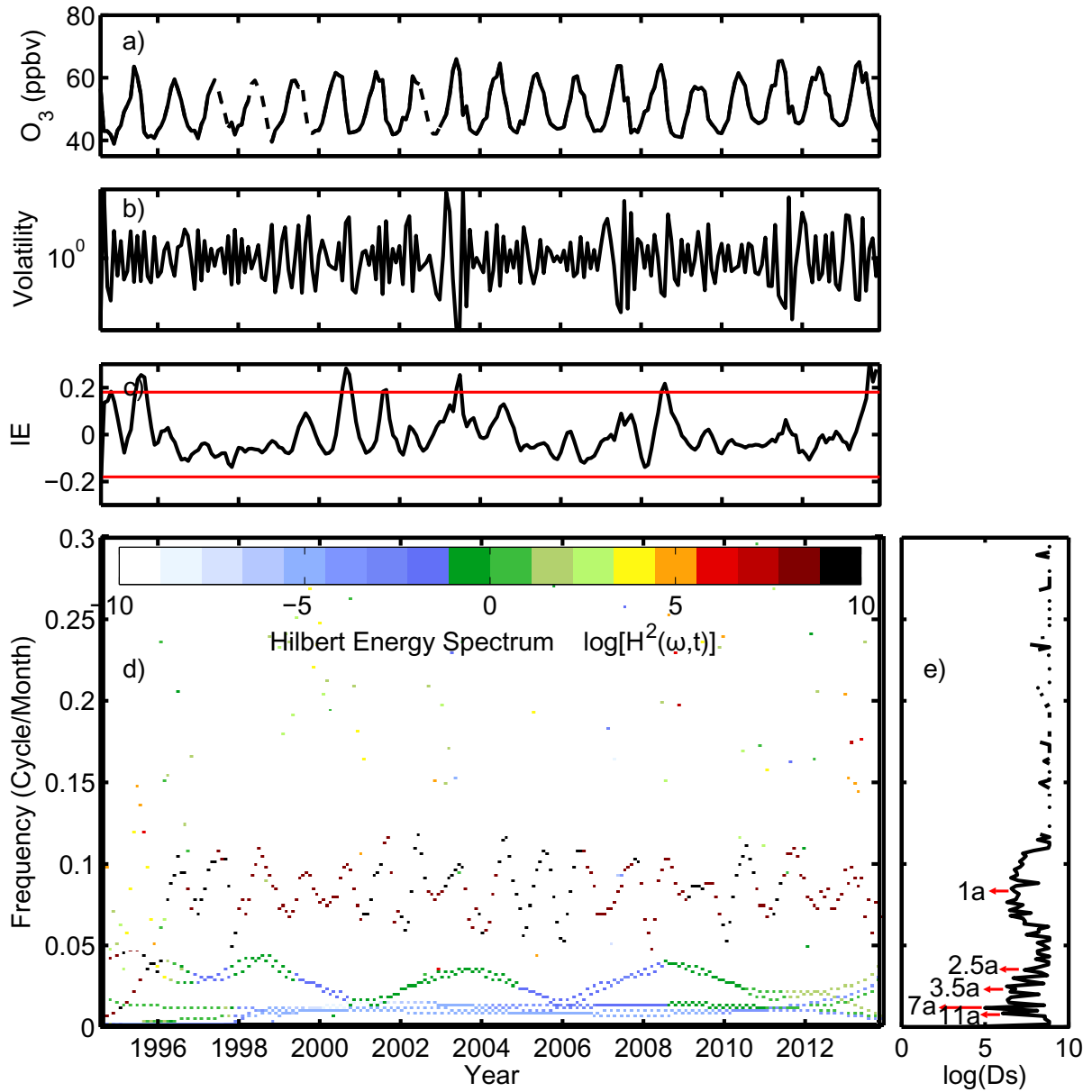
7



1
 2 Figure 7 a) The anomaly of the interpolated monthly average ozone (black line, with the
 3 dashed line segments representing values interpolated using the method in section 2.5), the
 4 sum of last IMF and the residual (c_5+r , red line), and the sum of the last two IMFs and the
 5 residual (c_4+c_5+r , blue line); b) the slope of the sum of last IMF and the residual (c_5+r , red
 6 line) and the sum of the last two IMFs and the residual (c_4+c_5+r , blue line).

7

1



2

3 Figure 8 The interpolated monthly average ozone mixing ratio signal at Mt. WLG during
4 1994-2013 (a), the volatility (b), the normalized mean value of the instantaneous energy (red
5 lines: $\pm 2\sigma$) (c), Hilbert Energy Spectrum (d) and the degree of stationarity (e).

6

7

8

9

10

1
2
3
4